The Pennsylvania State University

The Graduate School

College of Engineering

CALCULATION OF TEMPERATURES IN GAS TURBINE ROTOR-STATOR CAVITIES USING CONJUGATE HEAT TRANSFER

A Thesis in

Mechanical Engineering

by

Aneesh Sridhar Vadvadgi

Submitted in Partial Fulfillment
of the Requirements
for the Degree of

Master of Science

May 2010

The thesis of Aneesh Sridhar Vadvadgi was reviewed and approved* by the following:

Savas Yavuzkurt
Professor of Mechanical Engineering
Thesis Advisor

Anil K. Kulkarni
Professor of Mechanical Engineering

Karen A. Thole
Professor of Mechanical Engineering
Head of the Department of Mechanical and Nuclear Engineering

*Signatures are on file in the Graduate School

ABSTRACT

The present study deals with the numerical modeling of the turbulent flow in a rotor-stator cavity with or without imposed through flow with heat transfer. The commercial finite volume based solver, ANSYS/FLUENT is used to numerically simulate the problem. A conjugate heat transfer approach is used. The study specifically deals with the calculation of the heat transfer coefficients and the temperatures at the disk surfaces. Results are compared with data where available. Conventional approaches which use boundary conditions such as constant wall temperature or constant heat flux in order to calculate the heat transfer coefficients which later are used to calculate disk temperatures can introduce significant errors in the results. The conjugate heat transfer approach can resolve this to a good extent. It includes the effect of variable surface temperature on heat transfer coefficients. Further it is easier to specify more realistic boundary conditions in a conjugate approach since solid and the flow heat transfer problems are solved simultaneously. However this approach incurs a higher computational cost. In this study, the configuration chosen is a simple rotor and stator system with a stationary and heated stator and a rotor. The aspect ratio is kept small (around 0.1). The flow and heat transfer characteristics are obtained for a rotational Reynolds number of around 10^6. The simulation is performed using the Reynolds Stress Model (RSM). The computational model is first validated against experimental data available in the literature. Studies have been carried out to calculate the disk temperatures using conventional non-conjugate and full conjugate approaches.

It has been found that the difference between the disk temperatures for conjugate and non-conjugate computations is 5 K for the low temperature boundary conditions and 30 K for the high temperature boundary conditions. These represent differences of 1% and 2% of the respective stator surface temperatures. Even at low temperatures, the Nusselt numbers at the disk surface show a difference of 5% between the conjugate and non-conjugate computations, and far higher

at higher temperatures. It has also been found that the Reynolds Stress Model (RSM) is the most appropriate one for such kind of swirling flows with heat transfer. RSM can be used for all boundary conditions for swirling flows to produce very satisfactory results. The other models such as k-ε, k-ε Realizable and SST k-ω produce good results only for certain specific cases.

TABLE OF CONTENTS

LIST OF FIGURES

NOMENCLATURE

Ek = Ekman number = $1/(G^2 Re)$

G = gap ratio = H/R

H = axial clearance between rotor and stator (m)

k = thermal conductivity (W/mK)

Nu = Nusselt number

Q = volume flow rate (m^3/s)

q = Rossby number = $Q/(2\pi\Omega R^2 H)$

Re = rotational Reynolds number = $(\Omega R^2)/\nu$

R = outer radius of the disks (m)

r = radial coordinate (m)

r^* = dimensionless radial coordinate

T = temperature (K)

T^* = dimensionless temperature

U_θ = swirl (circumferential) velocity component (m/s)

U_r = radial velocity component (m/s)

u_θ = dimensionless swirl velocity component

u_r = dimensionless radial velocity component

Z = axial distance from mid clearance

z = dimensionless axial distance

Greek Letters

Ω = angular velocity of the rotor (rad/s)

ν = kinematic viscosity (m^2/s)

Subscripts

0 = pertaining to conditions at inlet

1 = pertaining to conditions at the stator surface

ACKNOWLEDGEMENTS

I would like to sincerely thank Prof. Savas Yavuzkurt for being an excellent mentor over the entire course of my MS thesis. His excellent balance of encouragement in the face of difficulty and guidance backed by his indubitable technical knowledge has been wonderful. By far the best aspect has been his ability to get the best out of me by making me thoroughly enjoy my work.

I also sincerely thank Prof. Anil Kulkarni for his inputs and his careful review of my thesis.

I would also like to thank Sushant Dhiman for the many times he has helped me understand the intricacies of ANSYS/FLUENT. His constant support has helped me achieve deadlines with ease and confidence.

Chapter 1

Introduction and Literature Review

The study of the fluid flow and heat transfer in rotating-stationary disk systems is one that has aroused a lot of interest due to the application of such systems in several engineering applications. Rotor-stator disc cavities are formed as a consequence of supporting the alternate rows of stationary and rotating blades in gas turbine engines as can be seen in figure 1-1. A single disk is shown in figure 1-2. The blades are arranged around this disk for both the rotor and the stator.

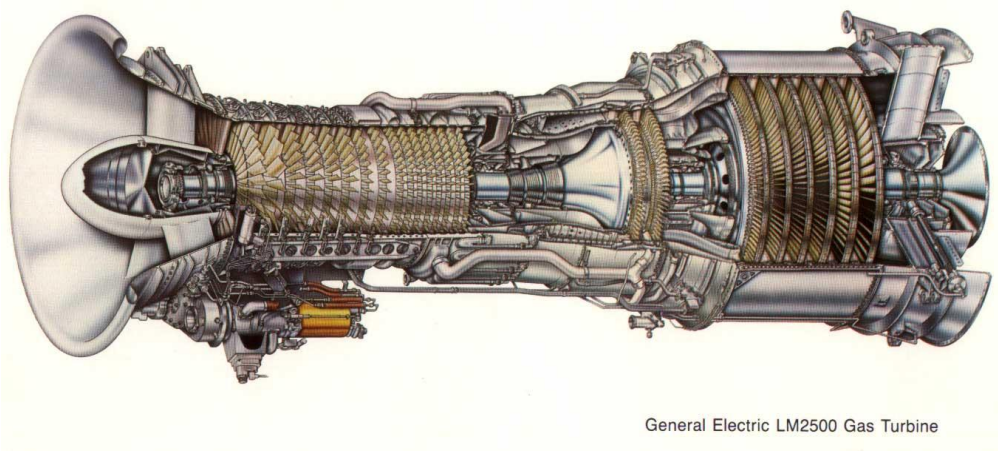

Figure 1-1 - General Electric LM2500 Gas Turbine **[1]**

An increase in efficiency of these systems can be brought about by increasing the operating temperature ratio by increasing the turbine inlet temperature. But this can only be done till a certain point, beyond which the metals will reach their melting points. Thus airflow is imposed between the rotor and stator to continually cool the rotor and stator and also the blades while they are operating. But the energy required to pump this air is a detriment to the efficiency. Hence, a proper understanding of the flow and heat transfer between a rotor and stator is required to

optimize the quantity of air flow used to cool the system. It is also important to know heat transfer more accurately for design of these components for reliability and longer life.

Figure 1-2 - A turbine disk **[2]**

Many research efforts have been directed towards this end over the past decade. Most of these efforts have been experimental. Daily and Nece **[3]** found that the flow structure between a rotor and a stator can be divided into two laminar and two turbulent regimes, with or without boundary layers. Djaoui et al. **[4]** performed experiments on an unshrouded rotor-stator system subjected to a superposed radial inflow. A shroud is an obstacle at the tips of the rotor and stator, usually put in to control outflow and to avoid unnecessary backflow. Simple sketches of shrouded and unshrouded rotor-stator systems are shown in figure 1-2.

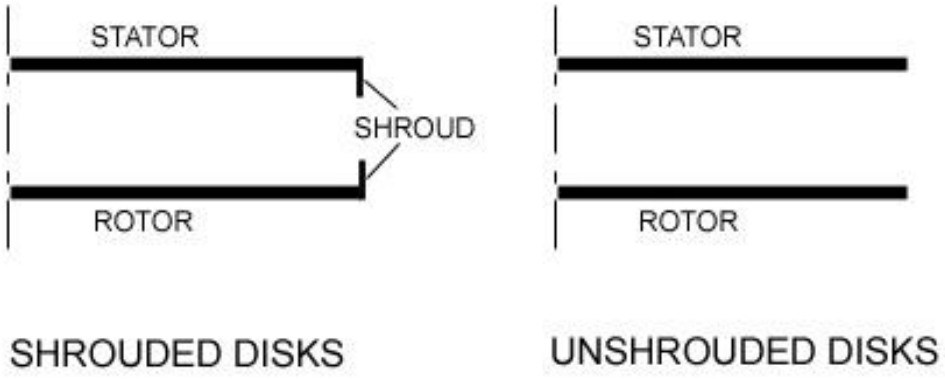

Figure 1-3 - General structure of shrouded and unshrouded disks

They presented the radial and circumferential velocity components, air temperature inside the cavity, temperature and temperature-velocity correlations, and also local Nusselt numbers on the heated stator. The gap ratio was kept small and the Ekman number corresponded to a turbulent regime with separate boundary layers. Poncet et al. **[5]** have explored Batchelor and Stewartson flow structures and the transition between the two in a high speed rotor-stator cavity with or without superimposed throughflow. They also validated the experimental work with numerical analysis using the Reynolds Stress Model. They found that the transition between the Batchelor flow and the Stewartson flow was characterized by the non-dimensional radial location and the modified Rossby number. Sparrow and Goldstein **[6]** performed experiments to obtain the local heat transfer coefficients along the heated shroud of a shrouded parallel disk system. The disks were superimposed with a coolant outflow and the temperature field within the enclosure formed by the disks and the shroud was also measured. They used relatively large aspect ratios ranging between 4/9 to 2 and rotational Reynolds numbers ranging from 0 to 10^6. Poncet et al. **[7]** validated the experimental work carried out by **[4]**,**[5]** and **[6]** by computationally simulating the same experiments using the Reynolds Stress Model to model the flow and found that the model agreed reasonably well with the experimental results. Beretta and Malfa **[8]** worked on the

specific case of an adiabatic rotor and an isothermal stator. They developed a semi-empirical model based on mass and angular momentum balances and the Reynolds analogy to evaluate the temperature fields and heat fluxes. They then validated the model by performing computations in FLUENT using the RNG k-ε model. Northrop and Owen **[9]** performed experiments on a rotating cavity with a radial outflow for a range of rotational Reynolds numbers up to 3.3×10^6, and validated the results with theoretical predictions. They used a gap ratio of 0.6. Faragher and Ooi **[10]** validated the experimental work of Northrop and Owen **[9]** by performing CFD analysis using k-ε turbulence model with the two-layer zonal model for near-wall treatment of Chen and Patel **[11]**. Roy et al. **[12]** performed experimental and computational studies on a model rotor-stator at rotational Reynolds numbers ranging from 4.65×10^5 to 8.6×10^5. The computations were carried out on FLUENT using the RNG k-ε turbulence model. Debuchy et al. **[13]** analyzed the asymptotic behavior of the motion of an incompressible fluid between a rotor and a stator with low aspect ratio superposed with a radial inflow and assuming a small Ekman number (Ek).

Very few research efforts have been directed towards modeling the flow and heat transfer between rotors and stators using a conjugate approach. The merits of the conjugate approach have been documented, for instance, by Kane and Yavuzkurt **[14]**. Roy et al. **[15]** computationally modeled the flow in an arbitrary shaped cavity using the realizable k-ε model in FLUENT, but their geometry did not have any throughflow. Yet another key aspect in this area is the choice of the turbulence model to solve the flow computationally. Since flows between rotor and stator falls under the category of rotational and separating flows, they require special models to accurately model them. Additionally, there is an imposed throughflow and heat transfer which are severe conditions for turbulence modeling methods. Iacovides and Chew **[16]** found out that the k-ε model with different wall treatments and the mixing length model are all inaccurate for modeling rotational flows. For the current computational analysis, the Reynolds Stress Model is

chosen which is derived from the Launder and Tselepidakis **[17]** model. Elena and Schiestel **[18**,**19]** have shown that this model is adequate in flows with rotation whereas the usual k-ε model is blind to any rotation effect and presents deficiencies. This model does not use the Boussinesq approximation and instead models all the Reynolds stresses independently.

Chapter 2

Objectives

The main objective of this study is to calculate heat transfer coefficients and disk temperatures using conventional (non-conjugate) and conjugate approaches in rotor-stator cavities and to show the differences in results. This will be studied for two cases – a high temperature case and a low temperature case.

A secondary objective is to ascertain the applicability of the Reynolds Stress Model provided by ANSYS/FLUENT to rotational flows with heat transfer, by comparing the CFD results with experimental data.

A further objective is to establish the best and most widely acceptable turbulence model which can be used to model swirling flows with heat transfer.

Chapter 3

Theory

Based on the suggestions in literature **[4,5,7]** as well as by ANSYS/FLUENT **[20]**, the Reynolds Stress Model (RSM) in ANSYS/FLUENT is used to solve the flow. This is the most elaborate RANS turbulence model that is provided by ANSYS/FLUENT. The main aspect of this model is that it does not employ the isotropic eddy-viscosity hypothesis. Instead it solves the transport equations for the Reynolds stresses along with an equation for the dissipation rate, in order to close the set of Reynolds-averaged Navier Stokes equations. As an example, the transport equation for the $\rho\overline{u_i'u_j'}$ term, as given in **[21]** is given below.

$$\underbrace{\frac{\partial}{\partial t}\left(\rho\overline{u_i'u_j'}\right)}_{Local\ Time\ Derivative} + \underbrace{\frac{\partial}{\partial x_k}\left(\rho u_k\overline{u_i'u_j'}\right)}_{C_{ij}\equiv Convection}$$

$$= \underbrace{-\frac{\partial}{\partial x_k}\left[\rho\overline{u_i'u_j'u_k'} + \overline{p\left(\delta_{kj}u_i' + \delta_{ik}u_j'\right)}\right]}_{D_{T,ij}\equiv Turbulent\ \ Diffusion}$$

$$+ \underbrace{\frac{\partial}{\partial x_k}\left[\mu\frac{\partial}{\partial x_k}\left(\overline{u_i'u_j'}\right)\right]}_{D_{L,ij}\ \equiv\ Molecular\ \ Diffusion} \underbrace{-\rho\left(\overline{u_i'u_k'}\frac{\partial u_j}{\partial x_k} + \overline{u_j'u_k'}\frac{\partial u_i}{\partial x_k}\right)}_{P_{ij}\ \equiv\ Stress\ Production}$$

$$- \underbrace{\rho\beta\left(g_i\overline{u_j'\theta} + g_j\overline{u_i'\theta}\right)}_{G_{ij}\ \equiv\ Buoyancy\ \ Production} + \underbrace{\overline{p\left(\frac{\partial u_i'}{\partial x_k} + \frac{\partial u_j'}{\partial x_k}\right)}}_{\phi_{ij}\equiv Pressure\ \ Strain}$$

$$- \underbrace{2\mu\overline{\frac{\partial u_i'}{\partial x_k}\frac{\partial u_j'}{\partial x_k}}}_{\varepsilon_{ij}\ \equiv\ Dissipation} \underbrace{-\ 2\rho\Omega_k\left(\overline{u_j'u_m'}\varepsilon_{ikm} + \overline{u_i'u_m'}\varepsilon_{jkm}\right)}_{F_{ij}\ \equiv\ Production\ \ by\ System\ \ Rotation}$$

$$+ \underbrace{S_{user}}_{User-Defined\ \ Source\ \ Term} \qquad (1)$$

Details about the various terms and constants can be found in **[23]**, **[25]** and **[26]**. Details about the modeling of each term are given in **[21]**. Of the three options to model the pressure term, the Linear Pressure-Strain Model derived from the proposals of Gibson and Launder **[23]**, Fu et al. **[22]** and Launder **[21,22]** is chosen for the present analyses as it provides far superior results over the other two models, namely the Quadratic Pressure-Strain and the Low-Re Stress-Omega models. It should be noted that despite the strong evidence in favor of RSM, these two other models – the Realizable and the k-ε models were also tested. The results were found to be unsatisfactory.

The Nusselt number is calculated by choosing cavity width H as the characteristic length. Following a standard procedure for the derivation of the Nusselt number, the expression for Nu on the stator becomes:

$$Nu = \frac{\mathrm{k_1 H}}{\mathrm{k_0 (T_1 - T_0)}} \frac{\partial \mathrm{T}}{\partial \mathrm{Z}} \left(\mathrm{r}, \frac{\mathrm{H}}{2} \right) \tag{2}$$

Chapter 4

Methodology

As noted above, the initial efforts of the study were devoted towards simulating experimental data available in literature using ANSYS/FLUENT code with the Reynolds Stress Model provided.

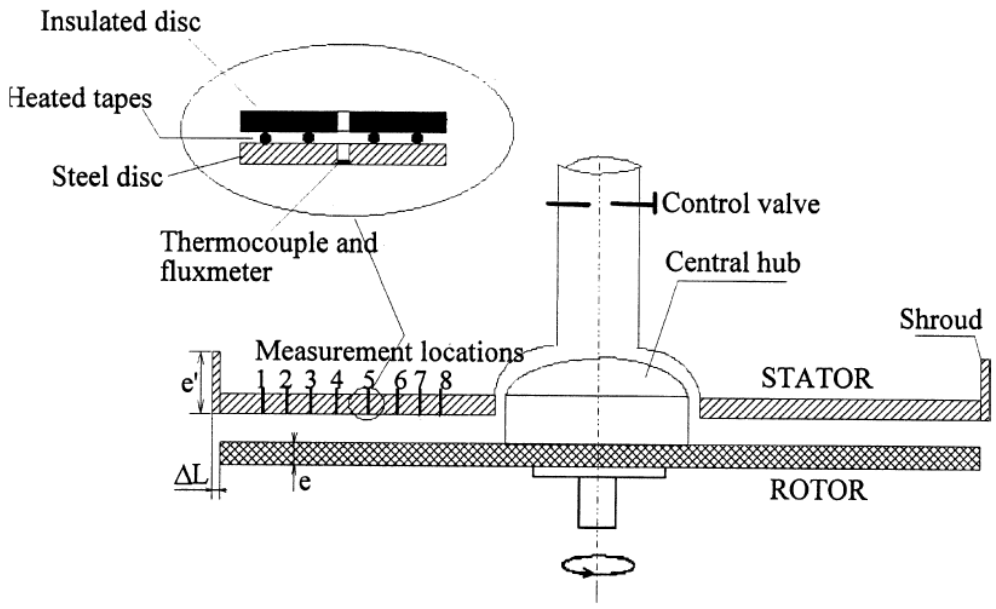

Figure 4-1 - Experimental Setup used by Djaoui et al. **[4]**

For this purpose, the experiment carried by Djaoui et al. **[4]** was chosen because it involved centripetal throughflow of air without any shroud in the path of the air, making the computation relatively simple. The accurate experimental data provided by the authors also aided the validation. The experimental setup used by Djaoui et al. **[4]** is shown in figure 1 above.

The fluid (air) enters the cavity between the rotor and stator at its periphery radially through the gap and leaves the system axially through the opening between the hub and the stator. The

throughflow is said to be centripetal. The stator is heated whereas the rotor is exposed to the ambient air. There is no shroud at the entry region blocking the inflow. The computational modeling is performed by taking an axisymmetric section of the system and solving it accordingly. This is done in order to save computational time. Since the air enters the inlet directly from the surrounding atmosphere, a uniform velocity profile is assumed at the inlet. For the present computations, G is 0.08 and rotational speed of the rotor is 1500 rev/min. This corresponds to a rotational Reynolds number of 1.44×10^{6}. The Rossby number (q) is 7.2×10^{-3}.

In the experiment carried out by Djaoui et al. **[4]**, the stator is heated on the outside by concentric heating tapes, the total power of which was 5.6 kW. The temperature distribution on the inside face of the stator was maintained as constant as possible up to $r^* = 0.88$ at 332 K and the temperature was measured by the use of copper-constantan thermocouples connected to electronic temperature controllers. Thus, in essence, the experiment has both conjugate and non-conjugate aspects. In order to validate the above experiment, two computations were carried out. The first one was a non-conjugate computation in which a constant temperature boundary condition was used for the inner surface of the stator. The second one was a conjugate computation in which a constant heat flux boundary condition was specified at the outer surface of the stator.

Boundary Conditions for the simulations were:

- *Inlet:* Velocity = 0.4239 m/s, Temperature = 297 K
- *Outlet:* Pressure outlet, open to ambient air at 297 K
- *Rotor:* Constant temperature of 297 K
- *Stator:* Constant temperature of 332 K on the inner surface for non-conjugate simulation, constant heat flux of 13641 W/m^2 on the outer surface for conjugate simulation.

- *Material of rotor and stator for conjugate simulations:* Steel of thickness 20 mm and with k = 16 W/mK

The conjugate and non-conjugate computations with the above mentioned boundary conditions are used for the purpose of comparing and verifying the validity of the computational approach only, since they have different boundary conditions due to the nature of the experimental setup. The two computations are compared independently with the experimental results and not with each other. In order to compare conjugate and non-conjugate approaches, the boundary conditions for both are kept identical as explained later. For clarity, these computations are referred to as "External BC" and "Internal BC", where BC stands for boundary conditions. Thus, the External BC refers to the conjugate computation and the Internal BC refers to the non-conjugate computation.

It should be noted that he grid used for the non-conjugate computation has zero thickness for the rotor and stator walls to save computational cost. The computations were carried out by following the suggestions listed in **[20]** for simulating rotational flow. Accordingly, the flow was first allowed to develop for zero rotational speed and then the rotational speed was slowly increased till the final value allowing the flow to develop at each stage. Also, at each stage, the momentum equation describing the swirl velocity, and the flow equations (continuity and momentum) were first allowed to develop separately for some time and then they were allowed to develop together. The details of the flow geometry and the coordinate system used for the computations are shown in figures 4-2 and 4-3 below.

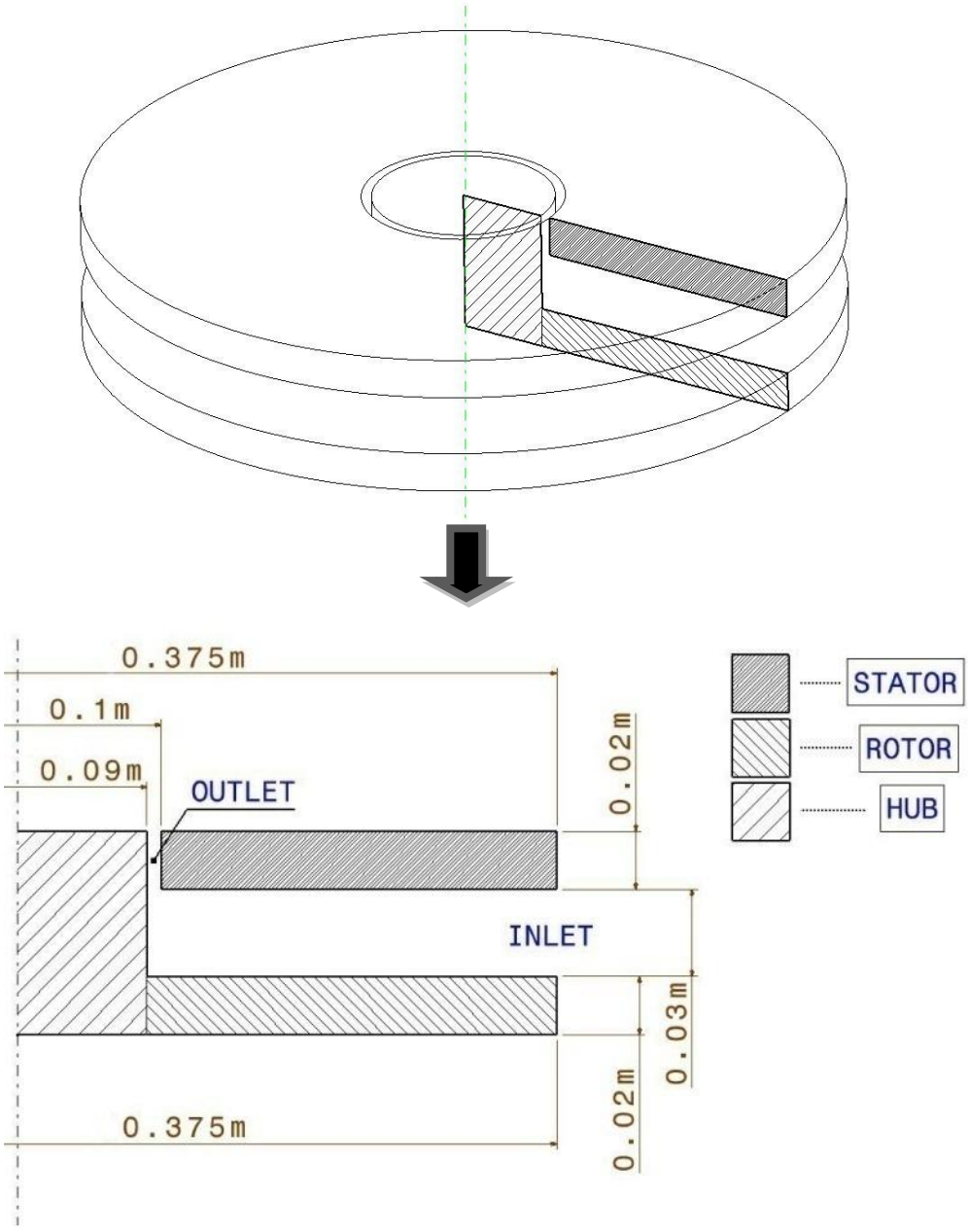

Figure 4-2 - Geometry used for computations

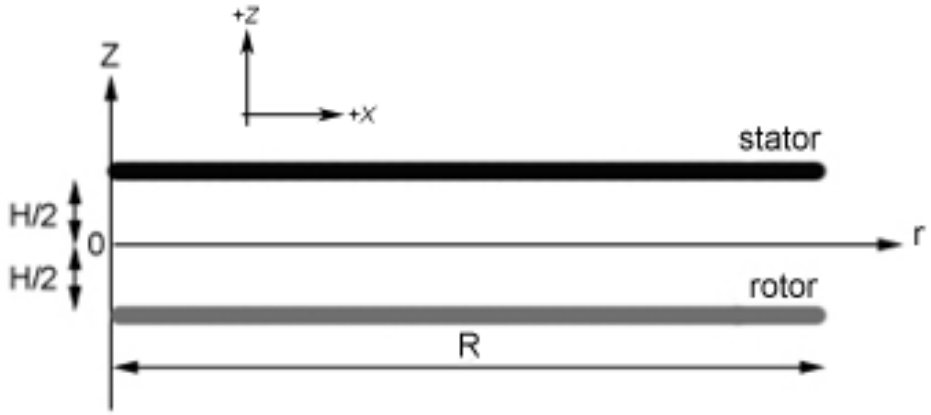

Figure 4-3 - Coordinate System

Convergence Criteria, Grid Information and Grid Independence Studies

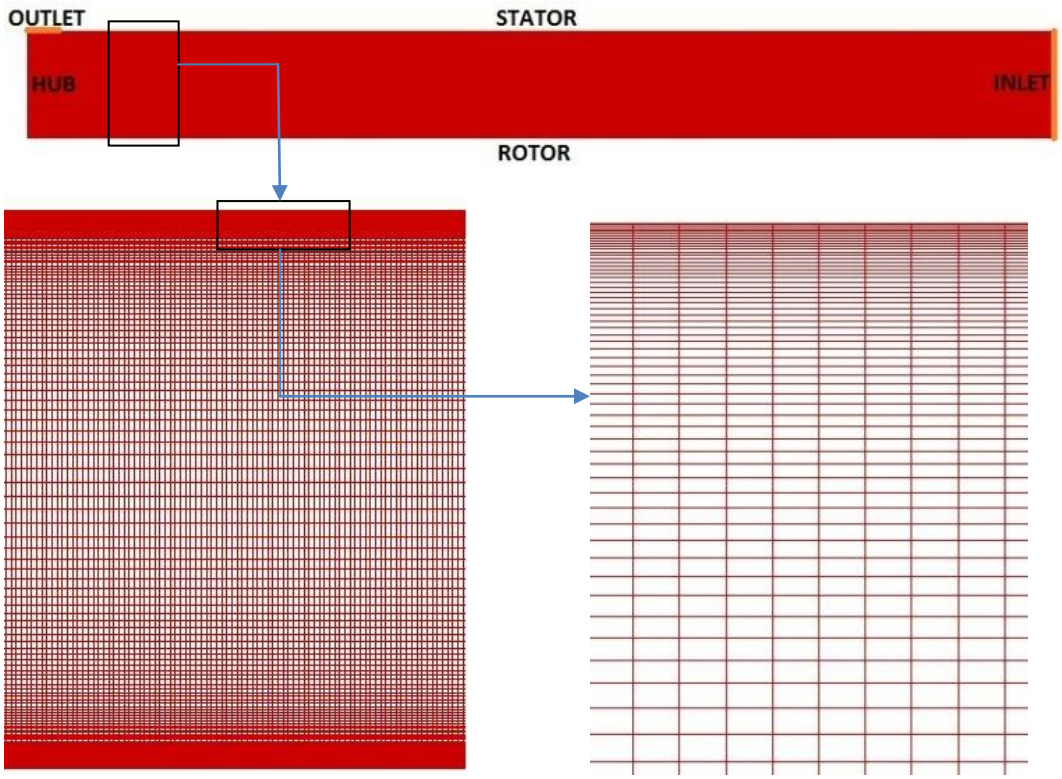

Figure 4-4 – Grid showing the details of the boundary layer

Convergence of $1 \times 10^{-6}$was achieved for the velocity, continuity and momentum terms; and $1 \times 10^{-9}$for the energy terms. These values represent 3 orders of magnitude better than the ones suggested by ANSYS/FLUENT. A flux report of the mass flow rate over the whole domain was also computed and was found to be well within the convergence criteria set.

The grid used has a boundary layer grid attached to the rotor and stator surfaces with a first cell height of $1 \times 10^{-5}\ m$. It is a structured grid with 184408 quadrilateral cells. The details of the grid used are shown above in figure 4-4. In order to ascertain the credibility of the grid with regards to obtaining the correct results, grid independence studies were carried out. The criterion upon which the studies are based is the first cell height of the boundary layer, because this is the crucial region where momentum transfer occurs between the rotor and the fluid, and heat transfer occurs between the stator and the fluid. Grids of the same structure but with first cell heights of $5 \times 10^{-5}\ m$ and $2.5 \times 10^{-5}\ m$ were chosen. It should be noted that all the cells of the boundary layer are affected by the first cell height because the boundary layer grows at a fixed ratio with the first cell as the base. These corresponded to 94506 (verification grid 1) and 116889 (verification grid 2) quadrilateral cells respectively.

A very good indicator of the adequacy of the boundary layer is plot of the wall y^+ values. Figure 4-5 below shows the y^+ values along the rotor and stator walls. As shown by the plot, the wall y^+ is less than 1 for a large majority of the rotor and stator walls and never goes beyond 1.6. These are in accordance with the standard accepted norms.

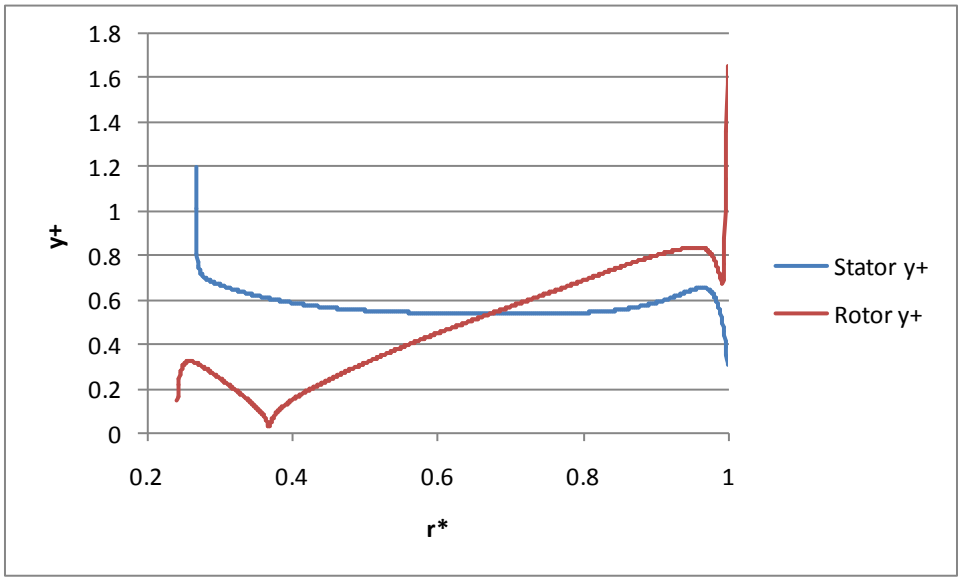

Figure 4-5 - Wall y+ values at rotor and stator

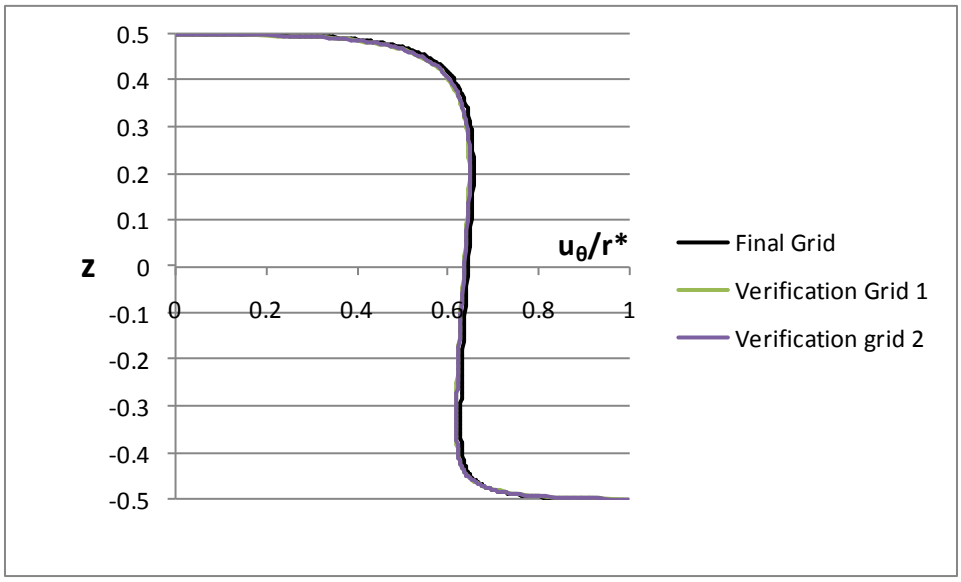

Figure 4-6 - Non dimensional swirl velocity vs axial distance at r* = 0.53

The results between the coarsest grid (first cell height of $5 \times 10^{-5}\ m$) and the finest grid (first cell height of $1 \times 10^{-5}\ m$) differed by only 1%. It is felt that this is a very good indication of the grid independence. Sample plots showing the swirl velocity and temperature distributions

at $r^* = 0.53$ for all the three grids are shown in figures 4-6 and 4-7. The non-dimensional quantities in the two figures are described in equations (3), (5) and (6) below.

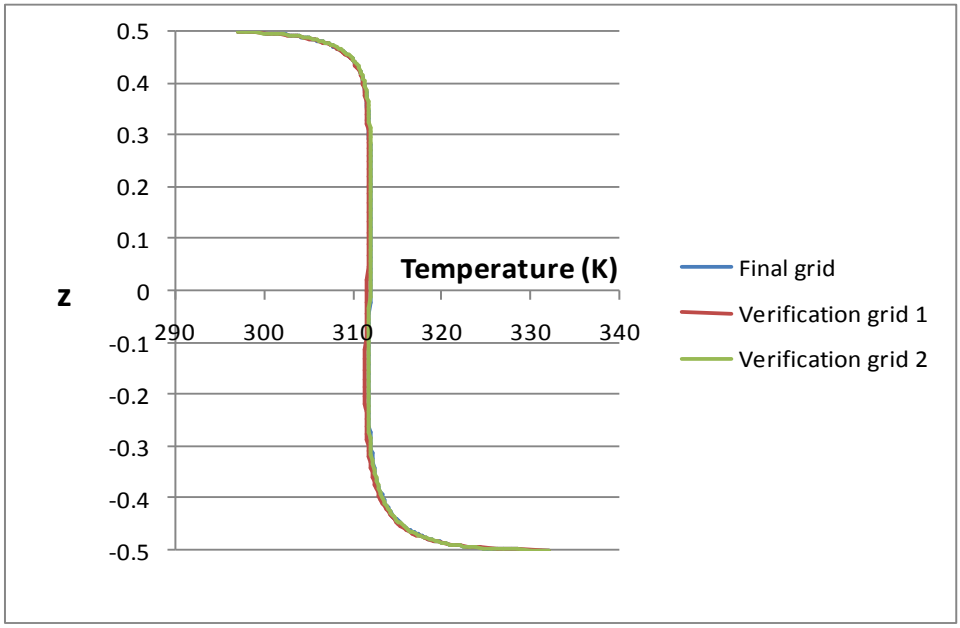

Figure 4-7 - Temperature in the cavity vs axial distance at r* = 0.53

Chapter 5

Results and Discussions – Verification of Computational Technique

The non-dimensional terms used in analysis below are defined as follows:

$$r^* = \frac{r}{R} \tag{3}$$

$$T^* = \frac{(T - T_0)}{(T_1 - T_0)} \tag{4}$$

$$z = \frac{Z}{GR} \tag{5}$$

$$u_\theta = \frac{U_\theta}{\Omega R} \tag{6}$$

$$u_r = \frac{U_r}{\Omega R} \tag{7}$$

Flow Field

Figure 5-1 shows the streamline pattern that is developed for the Internal BC case. It was found that this streamline pattern is largely unchanged for different thermal boundary conditions as long as the flow boundary conditions are the same. One main region of recirculation can clearly be seen. The core of the recirculating region is near the entry region of the fluid. The recirculating region gets thinner as the inward throughflow becomes stronger, i.e., when radial velocity increases as the flow approaches towards the center. We also see the development of the centripetal boundary layer adjacent to the stator (Bödewadt layer) and the centrifugal boundary

layer adjacent to the rotor (Ekman Layer). Some of the fluid gets heated along the stator, flows through the axis of the cavity and exits, while some other part of the fluid gets carried by the rotor without getting heated along the periphery.

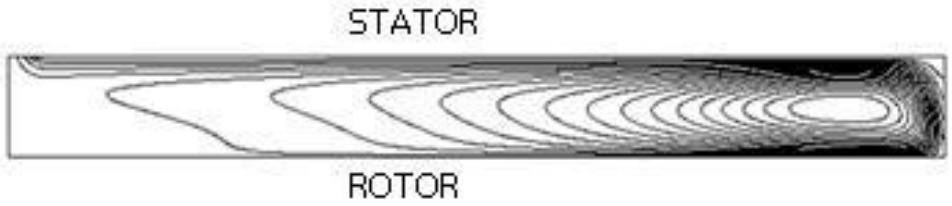

Figure 5-1 – Streamlines

Figure 5-2 shows the magnitudes and directions of the swirl velocities at various radial locations. Some regions of the figure have been magnified for clarity. We see that the magnitude of the swirl velocity in the mid plane of the cavity shows a decrease from the entry till a radial location corresponding to $r^* = 0.2$. Beyond this, the magnitude of the swirl velocity increases till the fluid exits. The rotor imparts angular momentum to the fluid, but since angular momentum is a function of radial distance, the quantity of angular momentum imparted by the rotor reduces with decreasing radial distance. Two contrasting processes occur in the fluid – the decrease of the angular momentum due to the reduction in the quantity imparted by the rotor; and the increase in the swirl velocity as the fluid moves inward towards the outlet as a consequence of the conservation of angular momentum (the radius and the area of cross-section of the fluid reduce as the fluid moves inward). Until a radius of about $r^* = 0.14$, the reduction in angular velocity due to decreasing angular momentum being imparted by the rotor dominates the increase in angular velocity due to the inward motion of the fluid. But, beyond this, the converse happens and the angular velocity increases till the outlet as a result. Another aspect of the flow structure is the change in the direction of the swirl velocity in the region near the rotor wall at a certain radius. This is once again caused due to the fact that the swirl velocity imparted by the rotor is a

function of the radius. At the rotor wall, due to the no-slip condition, the fluid has to have the same swirl velocity as the rotor. This keeps reducing with decreasing radial distance. At a radius of $r^* = 0.14$, the magnitude of the swirl velocity in the mid plane of the flow becomes higher than the magnitude at the rotor wall. Thus, the direction of the swirl velocity of the fluid, in the region near the wall, changes.

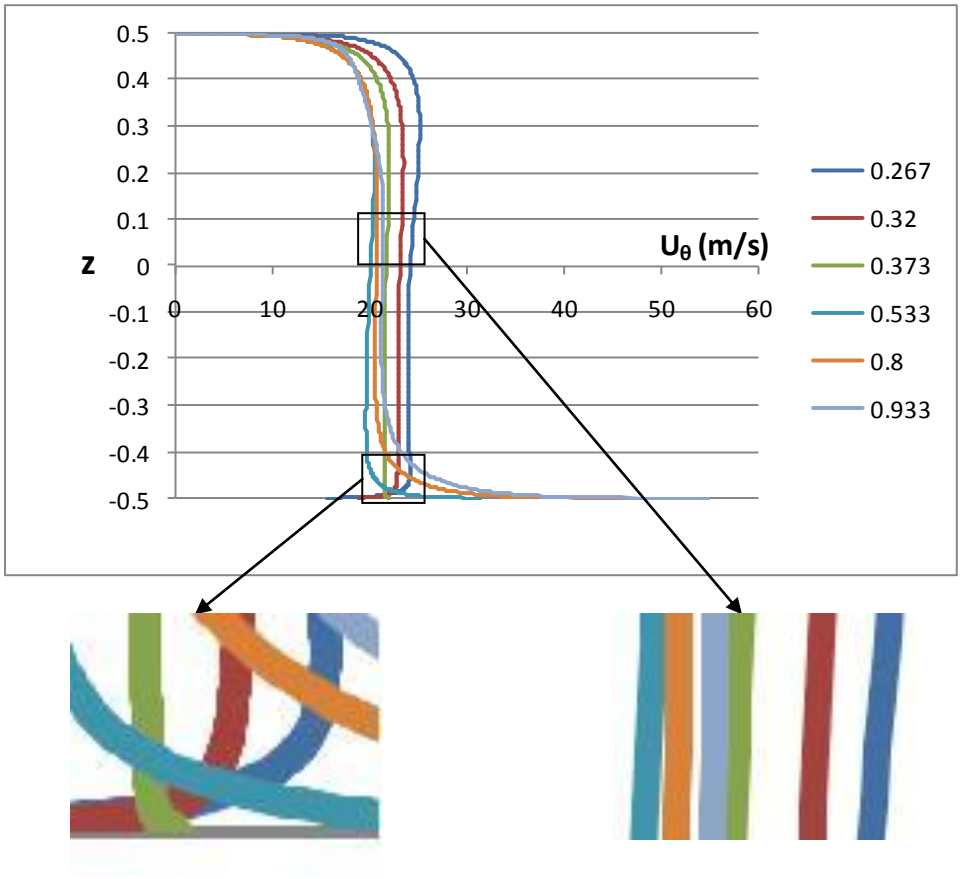

Figure 5-2 - Swirl velocities at various radial locations (r*)

Figure 5-3 shows the magnitudes and directions of the radial velocities at various radial locations. A change in the direction, similar to the one seen in the case of the swirl velocity is also seen for the radial velocity in the region near the rotor wall at a certain radius. When the fluid enters the cavity, the portion near the rotor is acted upon by a centrifugal force caused by the rotation of the rotor. The fluid enters the cavity radially

in the $-X$ direction. The centrifugal acceleration is in the $+X$ direction. Near the entry region the centrifugal acceleration is high. But as the fluid flows inwards, the centrifugal acceleration decreases since it is a function of the radius. At the same time, the radial velocity of the fluid in the $-X$ direction increases due to the conservation of mass, since the area of cross-section keeps reducing (in the three-dimensional flow geometry; not in the computational domain). Thus, at a certain radius, the inward acceleration of the fluid reverses the direction of the fluid flow in the region close to the rotor wall. This happens at a radius of $r^* = 0.14$.

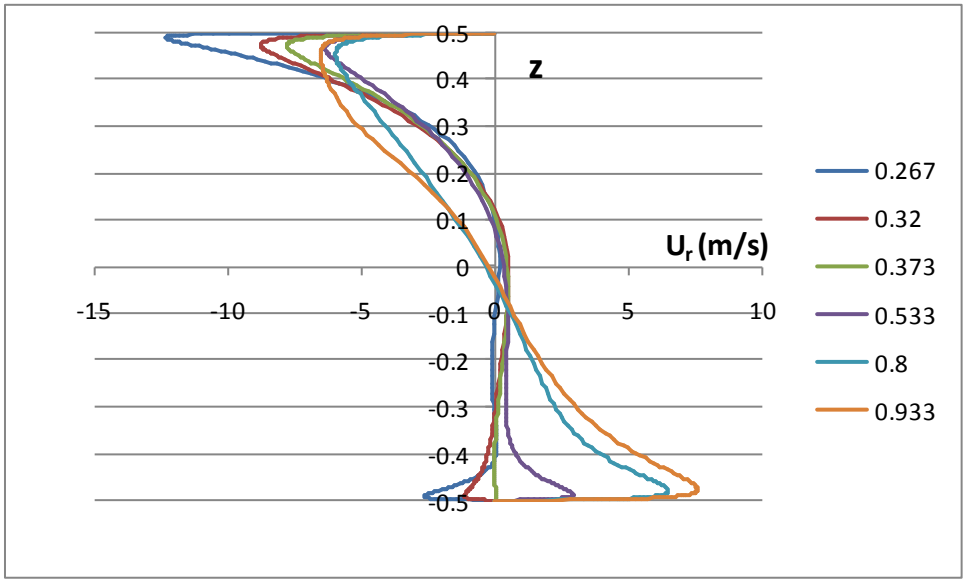

Figure 5-3 - Radial velocities at various radial locations (r*)

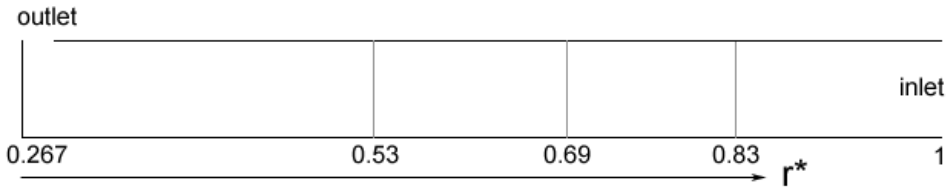

Figure 5-4 - Non-dimensional locations chosen for comparisons or data and computations

Figure 5-4 shows the three non-dimensional locations which are chosen to perform the flow and thermal field analysis below. These are the same measurement locations chosen by Djaoui et al. **[4]**.

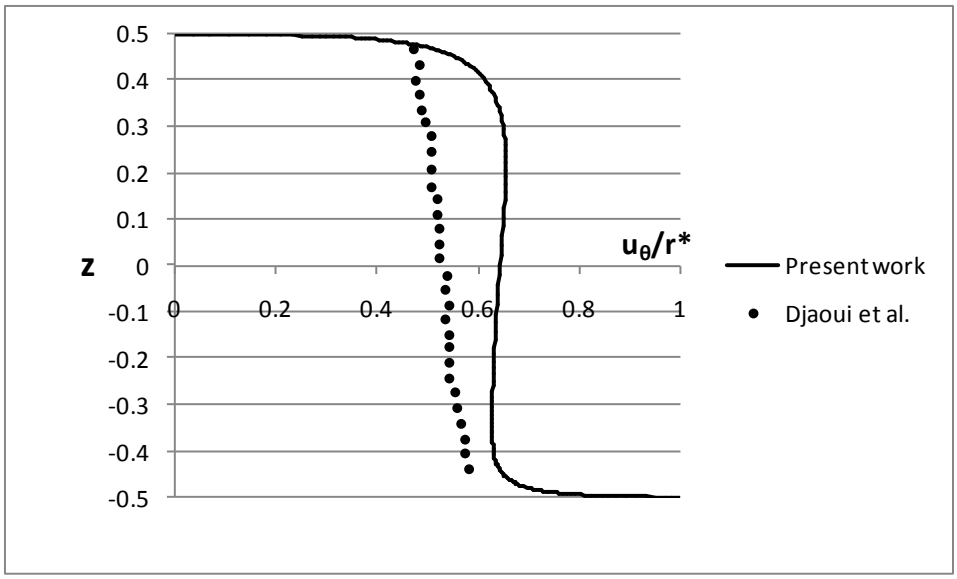

Figure 5-5 - Non dimensional swirl velocity vs axial distance at r* = 0.53, Re = 1.44×10^6 and q = 7.2×10^{-3}

Figures 5-5, 5-6, 5-7 and 5-8 show the non-dimensional swirl and radial velocity distributions in the axial direction at two radial locations. From these results it can be seen that the results of the computations are well matched with those of the experiment conducted by Djaoui et al. **[4]**. The trends match almost exactly and the magnitudes have a maximum deviation of 20% from the experimental results. These deviations could be explained by the fact that the thermocouples and flux meters used by Djaoui et al. **[4]** had an uncertainty of ±5% each, and also due to the fact that, as discussed before, the experiment conducted by Djaoui et al. was slightly different than the present simulations. For the complexity of the problem studied, it is thought that these are acceptable deviations. This gives us the confidence to believe that such a system can indeed be modeled in ANSYS/FLUENT by using the Reynolds Stress Model.

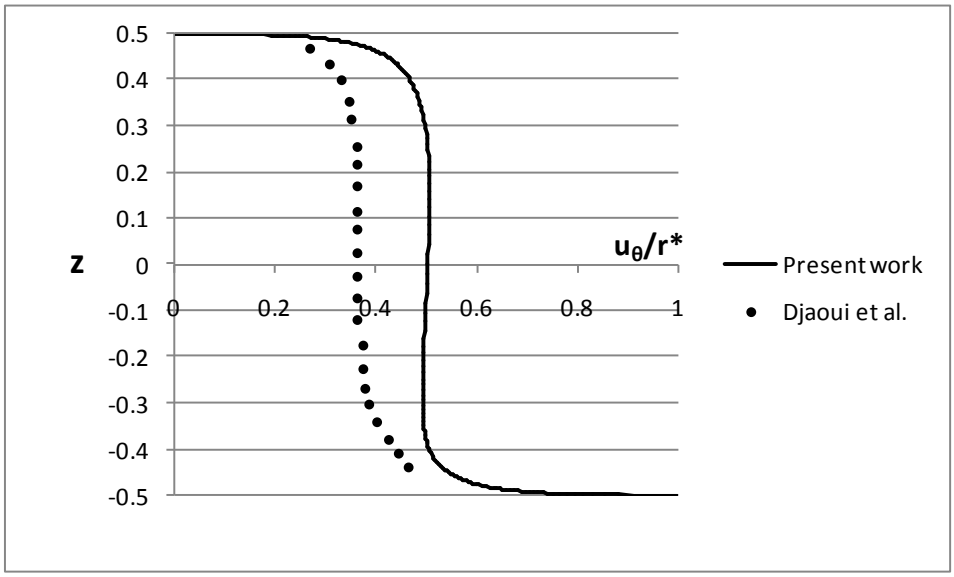

Figure 5-6 - Non dimensional swirl velocity vs axial distance at r* = 0.69, Re = $1.44x10^6$ and q = $7.2x10^{-3}$

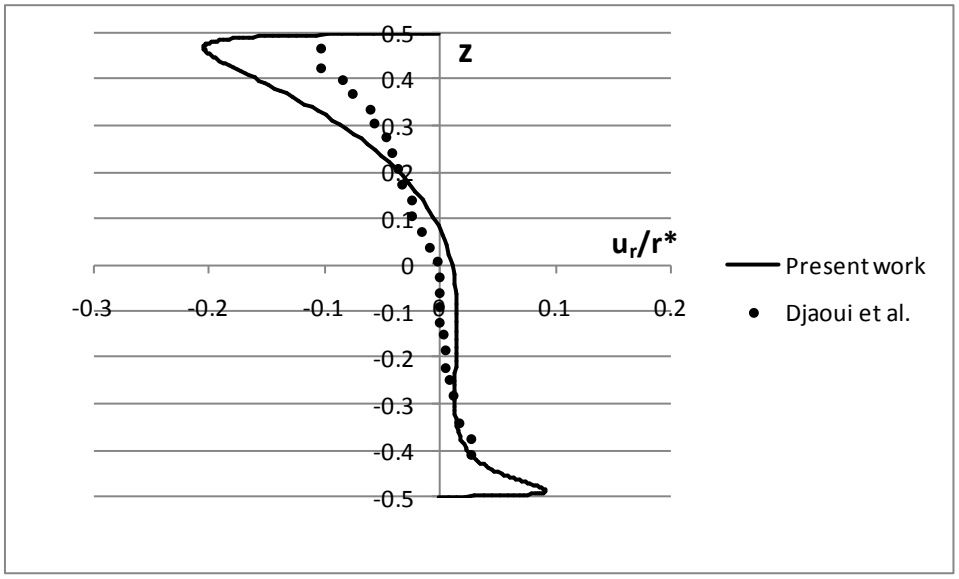

Figure 5-7 - Non dimensional radial velocity vs axial distance at r* = 0.53. Re = $1.44x10^6$ and q = $7.2x10^{-3}$

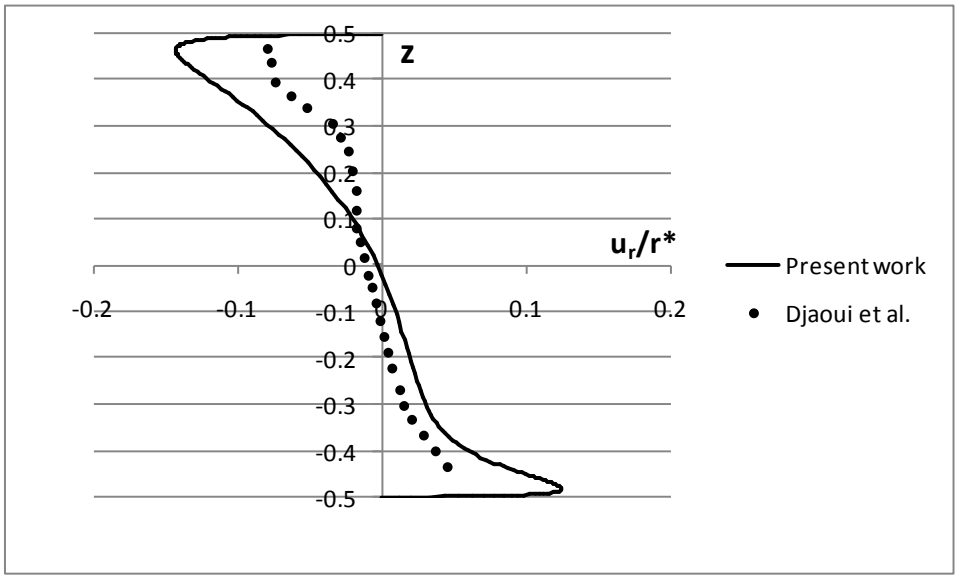

Figure 5-8 - Non dimensional radial velocity vs axial distance at r* = 0.69. Re = 1.44×10^6 and q = 7.2×10^{-3}

Temperature Field

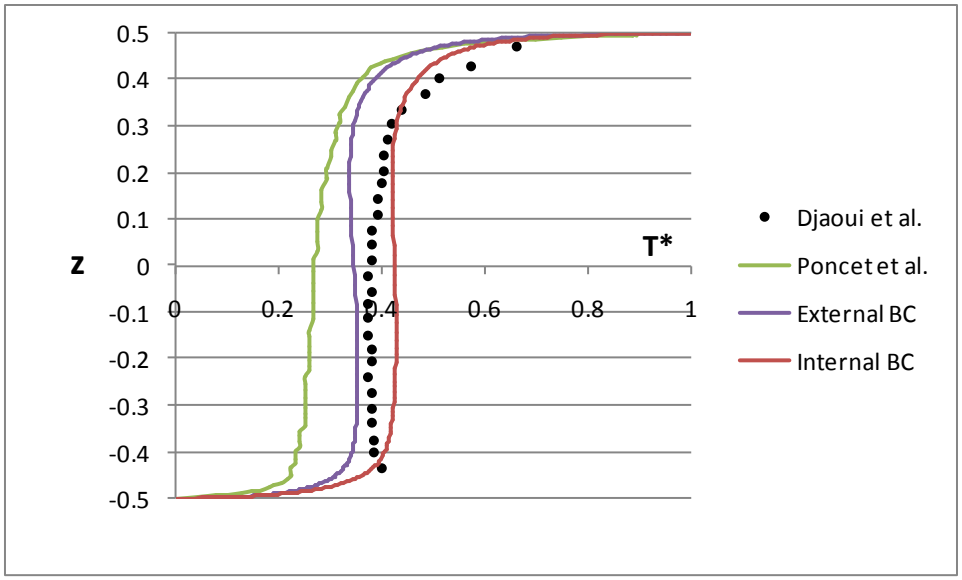

Figure 5-9 - Non dimensional temperature vs axial distance at r* = 0.53. Re = 1.44×10^6 and q = 7.2×10^{-3}

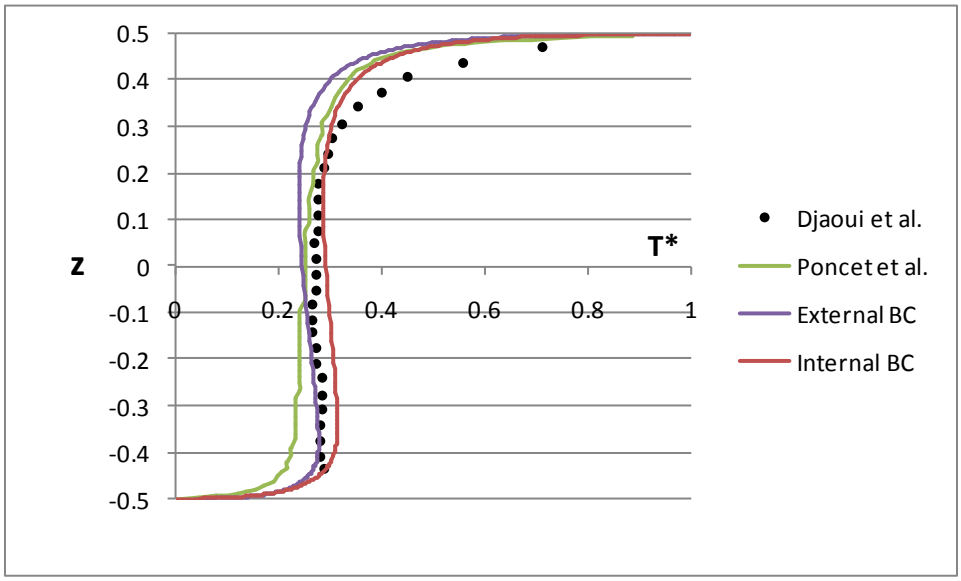

Figure 5-10 - Non dimensional temperature vs axial distance at r* = 0.69. Re = 1.44×10^6 and q = 7.2×10^{-3}

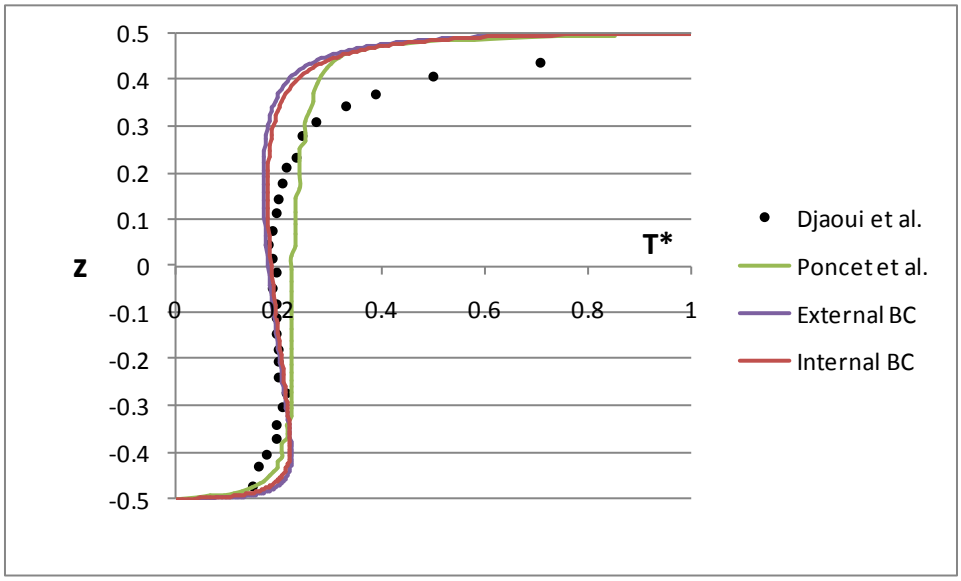

Figure 5-11 - Non dimensional temperature vs axial distance at r* = 0.83. Re = 1.44×10^6 and q = 7.2×10^{-3}

Figures 5-9, 5-10 and 5-11 show the axial variation of the non-dimensional temperature at three radial locations for the External BC and the Internal BC computations. Along with these,

the experimental results of Djaoui et al. **[4]** and computational results of Poncet et al. **[7]** (it should be recalled that Poncet et al. used the Reynolds Stress Model, but with some modifications) have also been shown.

Since constant temperature boundary conditions were specified at the rotor and the stator, it is no surprise to see the curves tending to 1 at the stator and 0 at the rotor in the non-dimensional plot due to the way T^* has been defined. The distribution of T^* in the region away from the walls is almost uniform. This is due to the fact that there is very good mixing of the flow due to the swirling and high turbulence and this causes the temperature to average out. Also, as the flow proceeds into the cavity, the value of T^*keeps on increasing. This is due to the fact that as the fluid proceeds inwards, more and more heat is transferred to it by the stator causing its temperature to rise, which causes $T^*$to rise.

Once again, the non-dimensional temperature distributions obtained by the computation match those obtained by experiment very well. These are also corroborated by the computational results of Poncet et al. **[7]** Another aspect to be observed is that, as mentioned before, the experiment carried out by Djaoui et al. **[4]** involved heating the stator from the outside, but at the same time, controlling the temperatures on the inner surface of the stator. Thus the experiment contains both conjugate and non-conjugate aspects in essence. Thus, it is not surprising to note that the conjugate and non-conjugate results from the computations, for the large part, fall on either side of the experimental results.

The disparity between the External BC and the Internal BC results increases as the fluid moves further inward into the cavity. This is because the effect of a conjugate calculation grows with distance from the entrance. Conjugate calculations cause change of the surface temperature

in the radial direction which leads to different heat transfer coefficients than a non-conjugate calculation.

Nusselt Number

Figure 5-12 shows the Nusselt number at the stator surface as a function of the non-dimensional radial distance. The External BC and Internal BC computations, as well as the experimental results of Djaoui et al. **[4]** and the numerical results of Poncet et al. **[7]** are shown. The External BC and Internal BC results compare well with the experimental data. The experiment data shows some scatter probably because, as stated by the authors, the thermocouples had an uncertainty of ±5%. They fall on either side of the experimental results due to the same reason as mentioned before. The difference between the two results grows as the fluid moves through the cavity as a result of the conjugate effect playing a stronger role with the passage of the fluid.

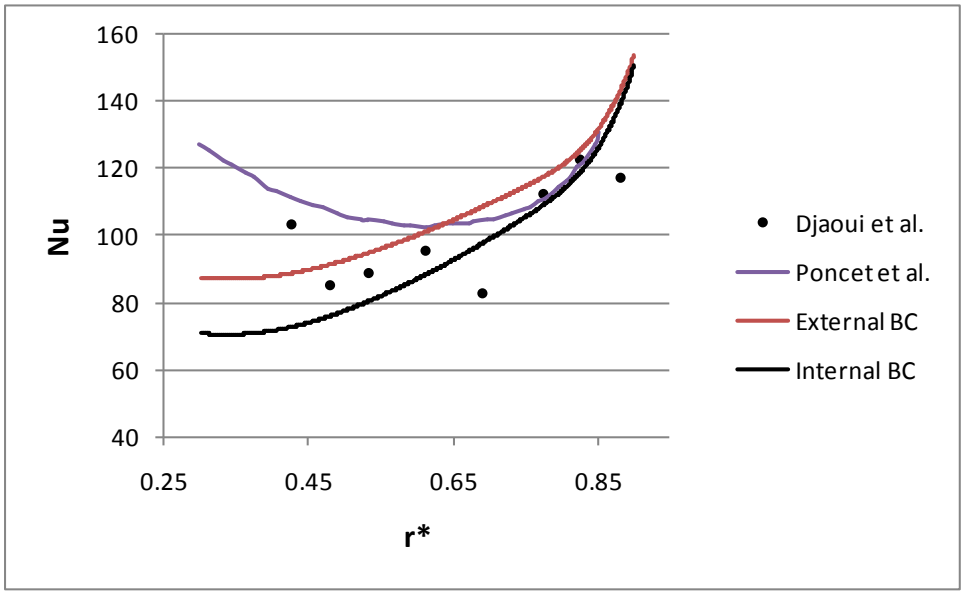

Figure 5-12 - Nusselt number at the stator surface vs non-dimensional radial distance

The Nusselt number is nearly the same in the entry region for both the External BC and Internal BC cases but, near the exit, the Nusselt number of the External BC case is about 25% higher than that of the Internal BC case. The Nusselt number is initially high in the entrance region of the fluid but falls as the fluid flows towards the exit. This is because in the entry region, the difference between the fluid and the stator temperatures is the highest and the boundary layer is very thin. This produces a high Nusselt number. But as the fluid proceeds in the cavity, its temperature increases and the difference between the stator and the fluid temperatures falls and with increasing boundary layer thickness, Nusselt numbers decrease.

Chapter 6

Results and Discussion – Comparisons between Conjugate and Non-Conjugate Approaches

As mentioned before, for the purpose of comparing conjugate and non-conjugate approaches for this configuration, separate computations were carried out where the boundary conditions for both the conjugate and non-conjugate computations are the same. The boundary conditions are:

- *Inlet:* Velocity = 0.4239 m/s, Temperature = 297 K
- *Outlet:* Pressure outlet, open to ambient air at 297 K
- *Rotor:* Constant temperature of 297 K
- *Stator:* Constant heat flux of 13641 W/m^2
- *Material of rotor and stator for conjugate:* Steel of thickness 20 mm and with k = 16 W/mK

For the conjugate computations, the boundary conditions specified for the rotor and stator refer to their external surfaces, with the 'coupled' boundary condition being applied at the inner surfaces. These two computations, with conditions given above are referred to as 'low temperature' computations in the discussions below.

Since it is expected that we would see better differences between the conjugate and non-conjugate approaches if the temperatures involved are higher, two computations, one conjugate and the other non-conjugate were carried out using the same grid but with the following boundary conditions:

- *Inlet:* Velocity = 0.4239 m/s, Temperature = 700 K
- *Outlet:* Pressure outlet, open to ambient air at 700 K
- *Rotor:* Constant temperature of 1400 K
- *Stator:* Constant temperature of 1600 K
- *Material of rotor and stator for conjugate:* Steel of thickness 20 mm and with k = 16 W/mK

These temperatures were chosen because they are close to the temperatures encountered in rotor-stator systems in turbines today **[27]**. The inlet velocity was maintained the same since the goal was to compare the effect of higher temperatures with the flow structure remaining very largely unchanged. These two computations are referred to as 'high temperature' computations in the discussion below.

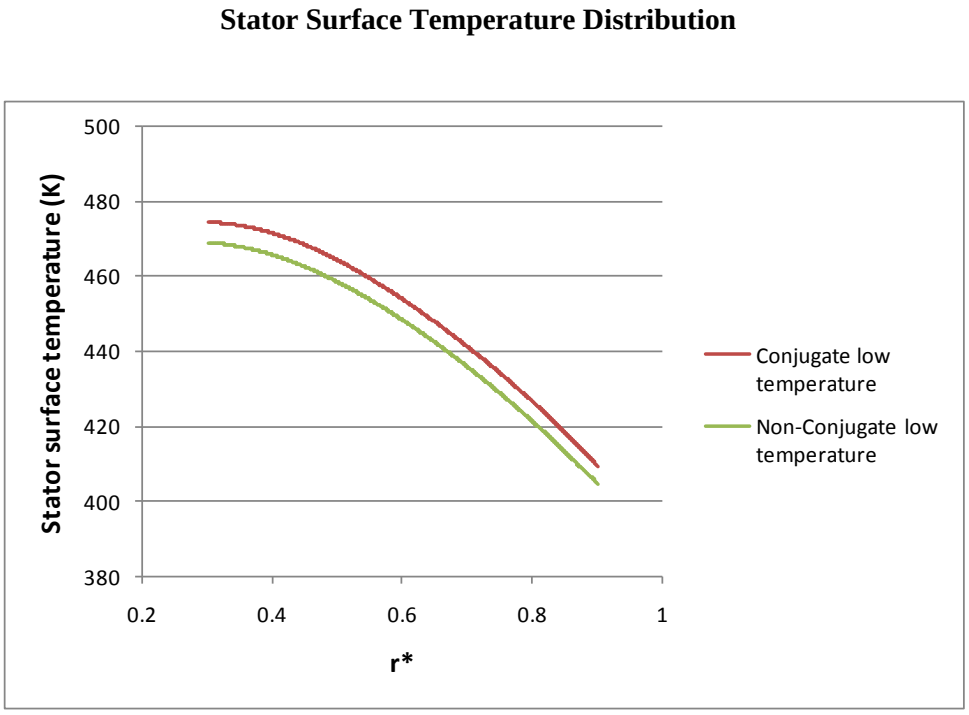

Figure 6-1 - Stator temperature vs non-dimensional radial distance for low temperature case

Figure 6-1 shows the temperature at the inner surface of the stator (adjacent to the fluid) as a function of the non-dimensional radial distance. We see that the stator surface temperature is higher for the conjugate computation when compared to the non-conjugate computation. The difference between the two is around 5 K, which is about 1 % of the non-conjugate stator temperature. In the conjugate case, the heat flows through the solid before entering the cavity and as a result the distribution of the convective heat transfer coefficient at the stator surface is affected. Due to this, the temperature distribution at the stator surface is affected. Thus we see that even for the relatively low temperatures encountered here, the difference in the stator temperatures between the conjugate and the non-conjugate cases is significant. Another implication of this result is the calculation of the coolant needs in a rotor-stator system. If the coolant needs were to be calculated based on the non-conjugate results, it could be underestimated because the stator temperature comes out higher for the conjugate case. Such an underestimation could lead to a potentially undesirable situation.

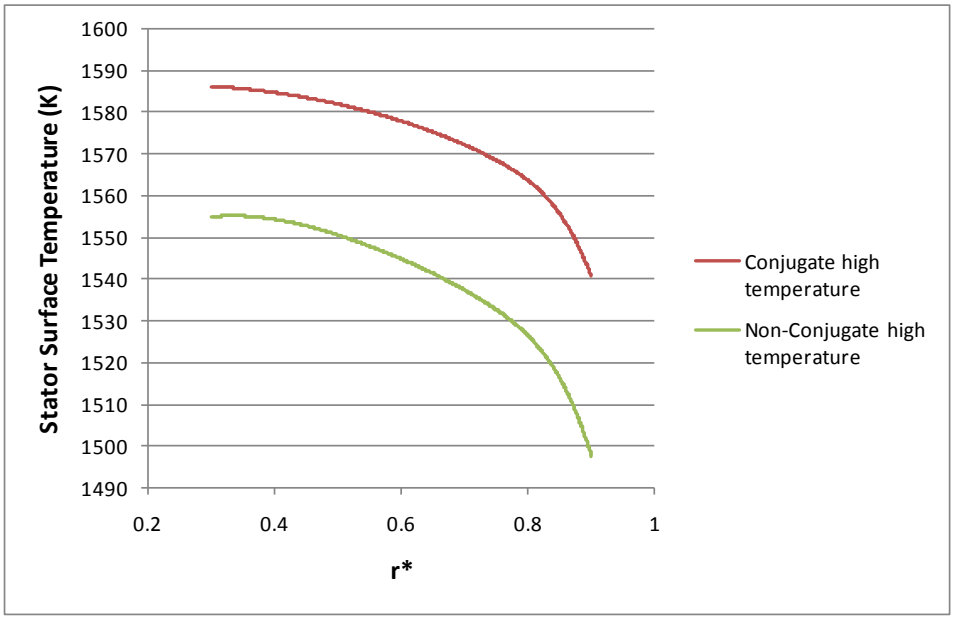

Figure 6-2 – Stator temperature vs non-dimensional radial distance for high temperature case

Figure 6-2 shows the stator surface temperature variation for the high temperature case. Again, we see that the stator surface temperature for the conjugate computation is higher than the non-conjugate computation. The important point to observe is that the temperature difference between the conjugate and the non-conjugate computations is higher here than the low temperature case. While the higher difference can be attributed to the higher operating temperatures, a difference of 30 K, as is the case here, is a very significant one. Even when expressed as a percentage of the non-conjugate stator temperature, the difference is about 2 %, which is higher than the low temperature case. Thus, we see that at higher temperatures, a conjugate computation is really important particularly at high turbine temperatures.

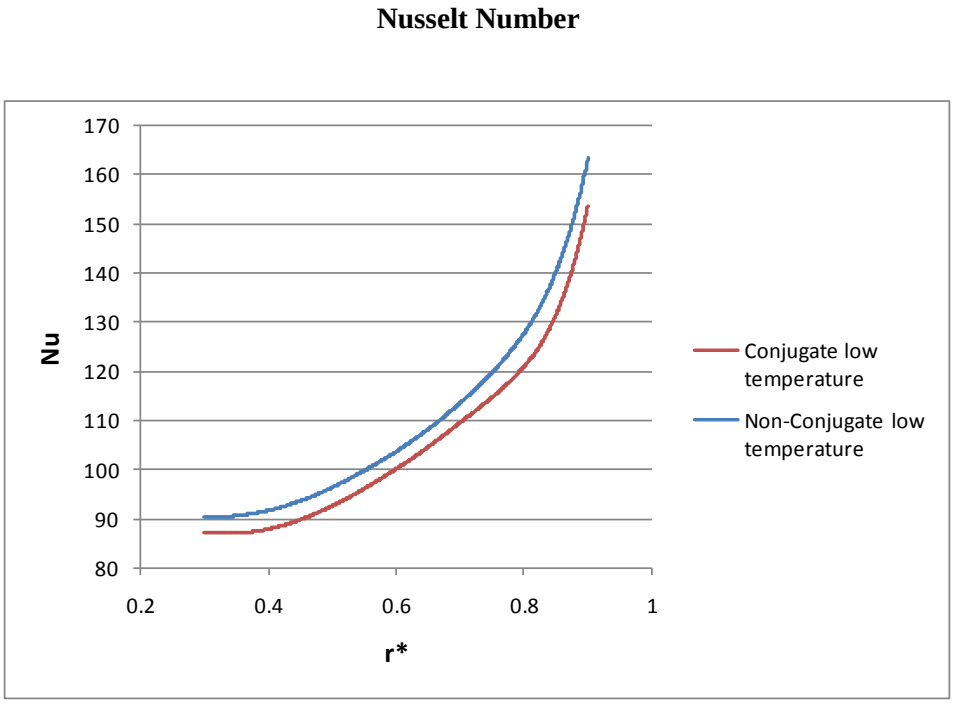

Figure 6-3 - Nusselt number at the stator surface vs non-dimensional radial distance for the low temperature case

Figures 6-3 and 6-4 show the Nusselt number at the stator surface as a function of the non-dimensional radial distance for the low temperature and high temperature cases respectively. As expected from the stator temperature data, the Nusselt number is higher for the non-conjugate computation. The lower Nusselt number in the conjugate computation leads to lesser heat transfer at the stator surface leading to higher temperatures as was seen. For the low temperature case, the Nusselt number for the non-conjugate computation is about 4.5% higher than the conjugate computation. For the high temperature case, the Nusselt number for the non-conjugate computation is dramatically higher than the conjugate computation. This is because, in equation (2), the $(T_1 - T_0)$ term is a large number for this case and any small change in the $(\partial T/\partial Z)$ term is magnified by the $(T_1 - T_0)$ term.

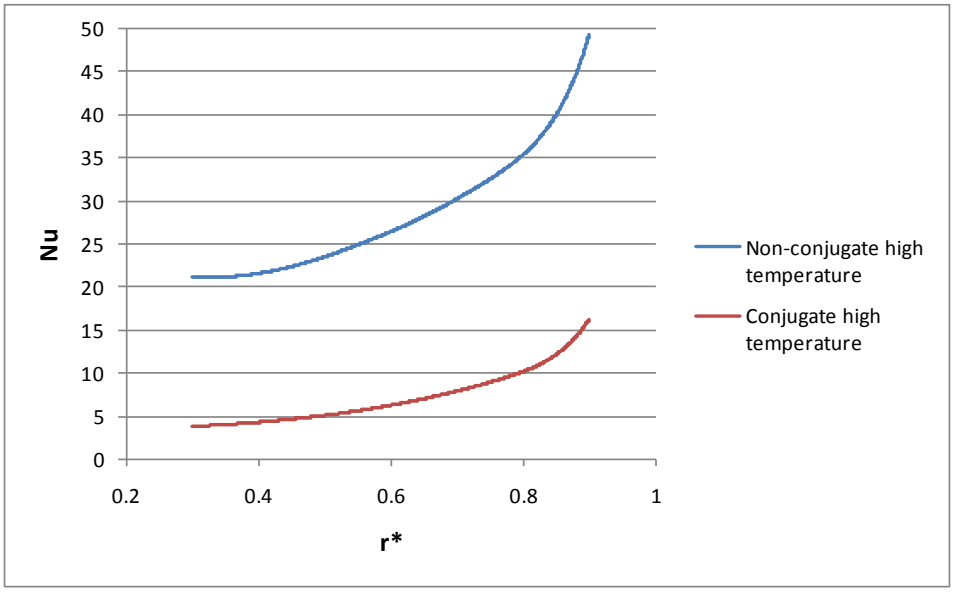

Figure 6-4 - Nusselt number at the stator surface vs non-dimensional radial distance for the high temperature case

Chapter 7

Exploration of the Iterative Conjugate Technique

An Iterative Conjugate Technique is a technique through which many non-conjugate computations are carried out and the results adjusted at each stage to effectively mimic a full conjugate computation. The technique is commonly used to separate the heat transfer phenomena in the fluid and the adjacent solid in a system. Doing so is very useful in certain situations where a full conjugate calculation is computationally very expensive. In other words, the full conjugate calculation may involve far too many cells. This type of procedure is also used by many gas turbine manufacturers.

In the present study, an iterative conjugate analysis was performed for the validation cases. This was done in order to explore the applicability of the Iterative Conjugate Technique to this problem as well as to ascertain the accuracy of the full conjugate computation. Since an iterative conjugate approach involves many non-conjugate computations, the results can be considered to be independent of the full conjugate approach.

The process is started by running a non-conjugate calculation with the same boundary conditions as mentioned previously. They are mentioned below again for lucidity:

- *Inlet:* Velocity = 0.4239 m/s, Temperature = 297 K
- *Outlet:* Pressure outlet, open to ambient air at 297 K
- *Rotor:* Constant temperature of 297 K
- *Stator:* Constant temperature of 332 K

The convective heat transfer coefficient along the stator surface is extracted from the calculation once it is completed. This is fed to a separate mesh made for heat transfer through the stator (shown in figure 7-1). The outer edge of the stator that is exposed to the ambient air is supplied with the constant temperature (332 K) boundary condition. This simulation is then run until convergence. The temperature profile thus produced at the inner edge of the stator, adjacent to the fluid is the result of the first iteration.

Now, this temperature profile is fed to the fluid and another non-conjugate computation is carried out to find new values of convective heat transfer coefficients along the stator. These are once again fed to the solid and computed to find the new temperature distribution along the fluid-stator interface. This completes the second iteration. This process is carried on until the temperature distribution along the stator surface converges and continuity of temperature and heat flux is achieved.

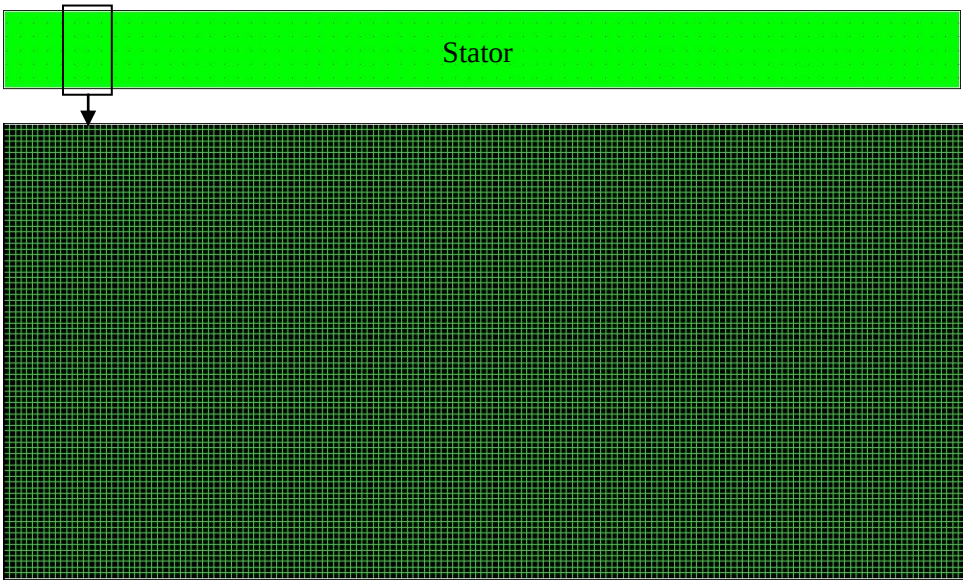

Figure 7-1 - Grid used for heat transfer through the stator

The results of the first and second iterations as well as the results of the full conjugate computations are shown in figure 7-2. As we clearly see, the results of successive iterations of the iterative conjugate technique tend to converge to the full conjugate results. This gives credibility to the results of the full conjugate calculation.

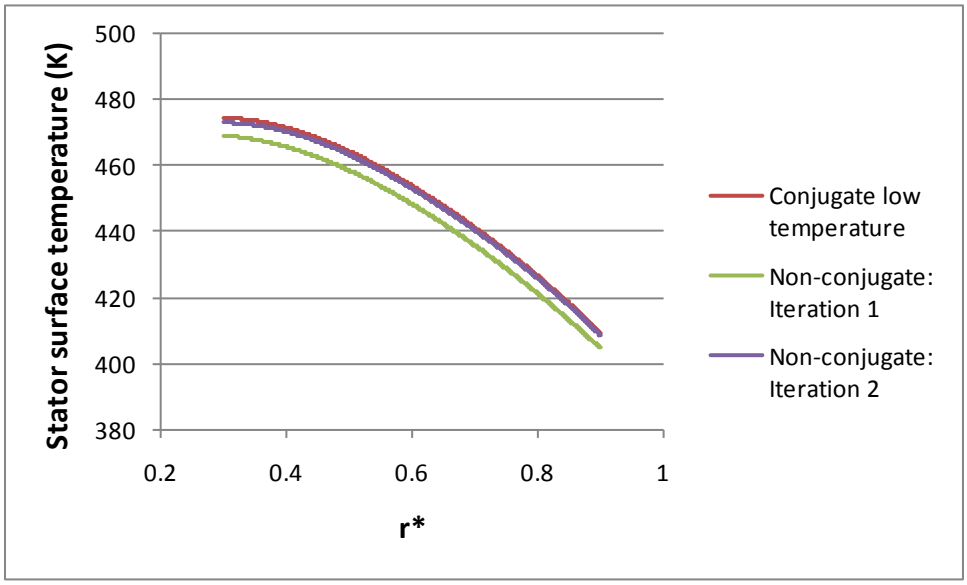

Figure 7-2 - Variation of Stator surface temperatures with non-dimensional radial distance for iterative and full conjugate apporaches

Chapter 8

Exploration of other Turbulence Models

As mentioned before, the Reynolds Stress Model has been used for all the computations in this study because it has been found to be the one that performs the best when swirling flows are encountered. But in order to ascertain how better this model performs when compared to other models, one simulation was performed using three other models:

- k-ε model
- k-ε Realizable model
- Shear Stress Transport k-ω model (SST k-ω)

Another reason for performing the simulations with other turbulence models is to try and find a model which produces results reasonably close to the RSM but at a cheaper computational cost. The RSM model as explained before, involves the simultaneous solution of 5 equations for 2-D flows. On the other hand, the k-ε, the k-ε Realizable and the SST k-ω models all involve only 2 equations for 2-D flows. The reduction in the number of equations is due to the fact that these models all use the Boussinesq approximation **[28]**. It basically involves relating the Reynolds stresses in the Navier Stokes equations for turbulent flow to the mean velocity gradients as:

$$-\rho\overrightarrow{u_i}\overrightarrow{u_j} = \mu_t\left(\frac{\partial u_i}{\partial x_j}+\frac{\partial u_j}{\partial x_i}\right)-\frac{2}{3}\left(\rho k+\mu_t\frac{\partial u_k}{\partial x_k}\right)\delta_{ij} \qquad (8)$$

where μ_t is the turbulent viscosity, k is the turbulent kinetic energy and all the other terms have their usual meaning. Further information about equation (8) or about any of the above mentioned models can be found in **[21]**.

The following two conjugate cases, which have already been run using RSM were simulated using the three above models. The high temperature case was run by employing variable properties.

Boundary Conditions for low temperature case:

- *Inlet:* Velocity = 0.4239 m/s, Temperature = 297 K
- *Outlet:* Pressure outlet, open to ambient air at 297 K
- *Rotor:* Constant temperature of 297 K
- *Stator:* Constant heat flux of 13641 W/m^2.
- *Material of rotor and stator for conjugate simulations:* Steel of thickness 20 mm and with k = 16 W/mK

Boundary Conditions for high temperature case:

- *Inlet:* Velocity = 0.4239 m/s, Temperature = 700 K
- *Outlet:* Pressure outlet, open to ambient air at 700 K
- *Rotor:* Constant temperature of 1400 K
- *Stator:* Constant temperature of 1600 K
- *Material of rotor and stator for conjugate:* Steel of thickness 20 mm and with k = 16 W/mK

Low Temperature Results

The flow, temperature and the Nusselt number results are shown below in figures 8-1, 8-2 and 8-3 respectively for the low temperature simulations. From the plot showing the variation of the non-dimensional swirl velocity at r* = 0.69, we see that surprisingly, the results of the other

three models seem to be better than the RSM since they compare better with the experimental results of Djaoui et al. **[4]**. Amongst the three models new models tested, it is very surprising to find that the best results are obtained by using the simplest of the three models, k-ε model. The other two models, SST k-ω and k-ε Realizable models follow the experimental data closely for the large part but are not as good as k-ε at some axial locations.

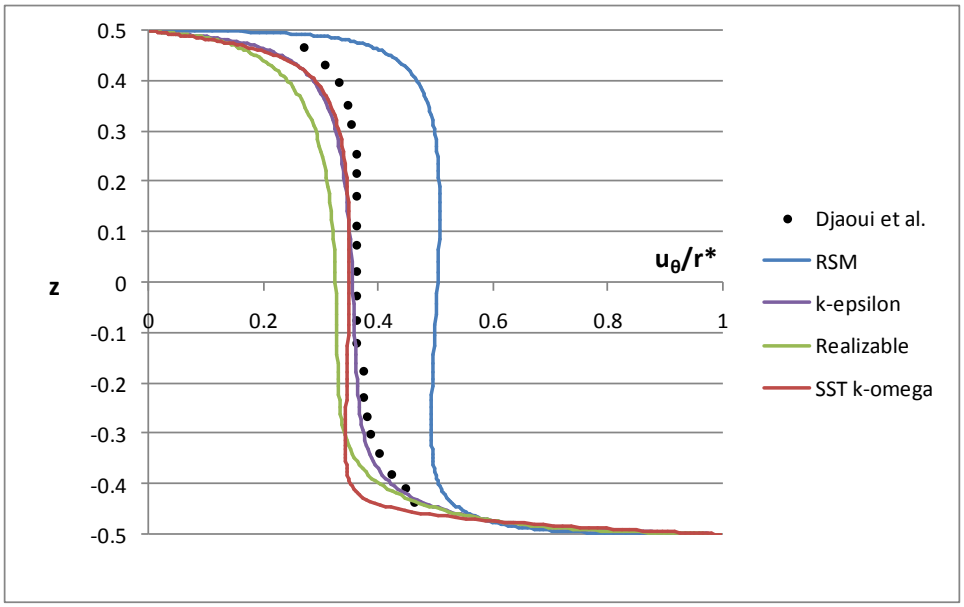

Figure 8-1 - Non dimensional swirl velocity vs axial distance for various turbulence models at r* = 0.69, Re = 1.44×10^6 and q = 7.2×10^{-3} (Low Temperature Case)

These results primarily highlight one aspect of the present flow. While it is true that the assumption that the Reynolds stresses are isotropic does not hold in general for flows with high swirl, the current case seems to have nearly isotropic Reynolds stresses. This is because the main difference between the three models considered and RSM is that the three models assume isotropic Reynolds stresses as part of the model while RSM does not. It is seen that the more complex models give worse results than the simplest one. This is probably because as the models become more complex, they become stiffer and not amenable to large types of flows. However,

concluding that the k-ε model is better just based on the flow results is erroneous. We also need to see how the different models perform for the thermal results. These are discussed below.

The stator surface temperature distribution and the Nusselt number distribution along the stator surface are shown below in figures 8-2 and 8-3.

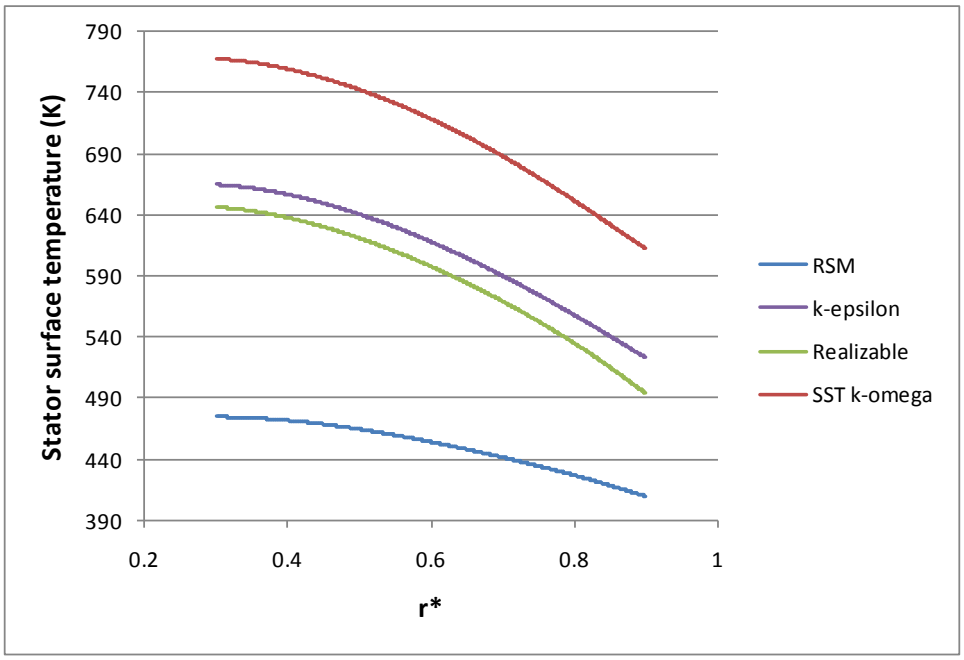

Figure 8-2 - Stator temperature vs non-dimensional radial distance for various turbulence models (Low Temperature Case)

We see that for predicting the thermal results, the RSM clearly outperforms the other three models which are based on the Boussinesq approximation. In fact, the stator surface temperatures predicted by the other three models are off by well over 50 %. This is also reflected in the Nusselt numbers along the stator surface. The other three models severely under predict the values of the Nusselt numbers. From this, we can infer that in the present case, while the Reynolds stresses may be nearly isotropic, the transport of heat in the fluid by turbulence is most certainly not isotropic. It needs to be modeled in the extensive way that RSM does in order to

obtain the correct prediction. Another inference that we can draw from these results is that, since the flow results produced from the other three models are good, it may be possible that the thermal results are wrong purely due to the fact that the turbulent Prandtl number used in these models may be wrong when they are applied to swirling flows with heat transfer.

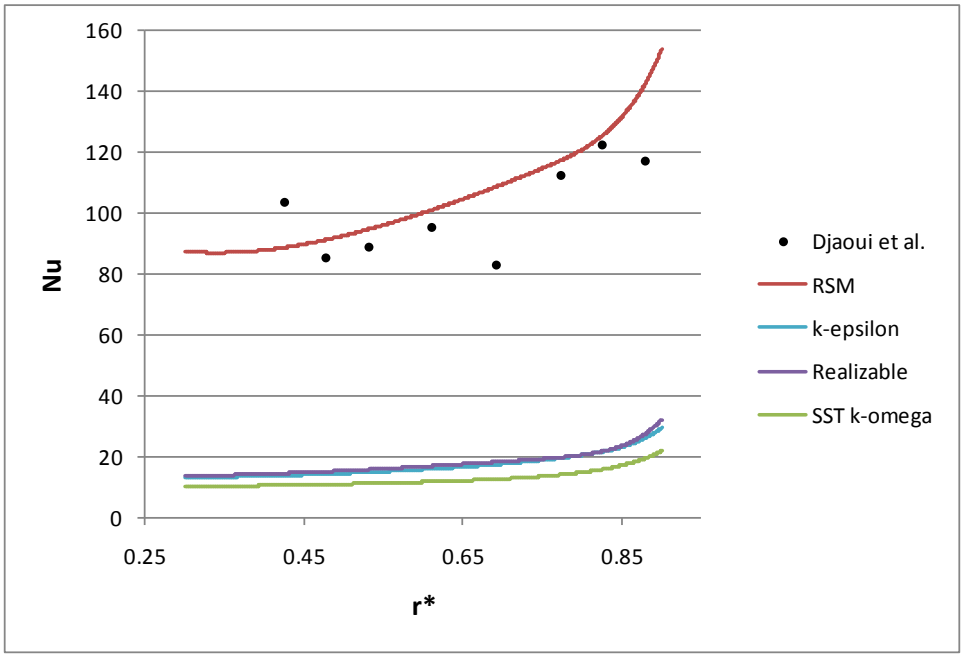

Figure 8-3 - Nusselt number at the stator surface vs non-dimentional radial distance for various turbulence models (Low Temperature Case)

Thus, on the whole, we can conclude that for the present boundary conditions, the RSM is still the best turbulence model to model flows of this nature, i.e., flows with high swirl and simultaneous heat transfer. Even though the flow results seem slightly better for the simpler models when compared to RSM, they perform very badly when it comes to predicting the thermal results.

High Temperature Results

The flow, temperature and the Nusselt number results are shown below in figures 8-4, 8-5 and 8-6 respectively for the high temperature simulations. It is seen that the flow results are quite similar to the low temperature case. The reason for this has been discussed before – the flow structures are not affected too much by temperature provided all other factors like the angular velocity of the rotor remain the same. Once again we see that the results of the three new cases are bunched together with the RSM results a little different. Based on the low temperature case where experimental results were available to be compared with, we can suspect once again that perhaps the three new cases do indeed predict the flow structures a little better than the RSM.

The discussions of the temperature and Nusselt number results are given below. A judgment can be made about the models only after taking these also into consideration.

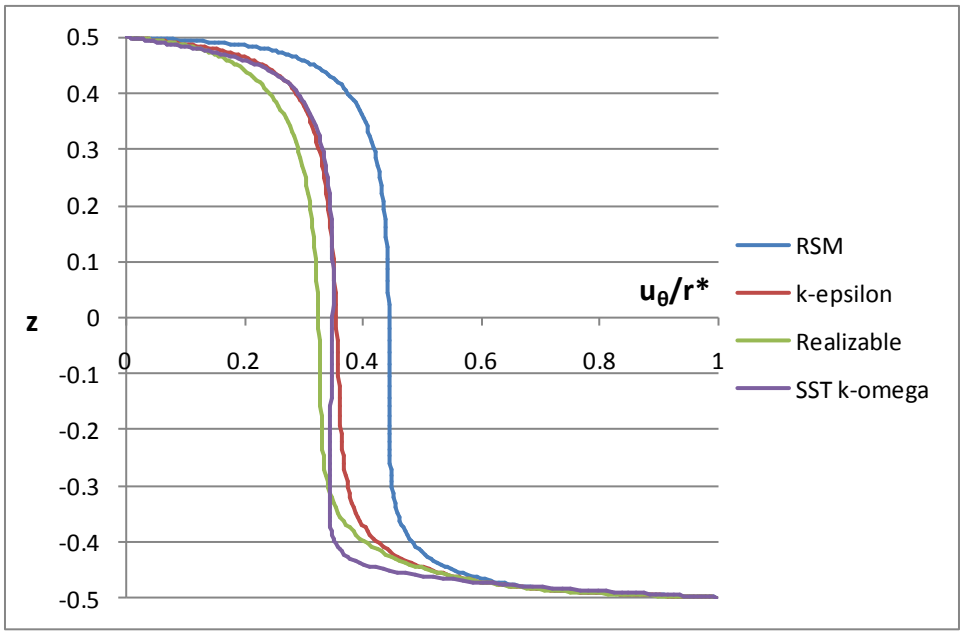

Figure 8-4 - Non dimensional swirl velocity vs axial distance for various turbulence models at r* = 0.69, Re = 1.44×10^6 and q = 7.2×10^{-3} (High Temperature Case)

From the plots below, it is observed that the distribution of the stator temperatures for this present simulation isn't as dramatically different between the models as was found in the low temperature case. In fact, the results of the k-ε, k-ε Realizable and RSM are largely the same with the SST k-ω model showing some deviation.

The reason why the other models are not dramatically different in this case is most probably because of the type of boundary condition specified here. In the low temperature case, a constant heat flux boundary condition was specified at the stator surface whereas in the high temperature case, a constant temperature boundary condition has been specified.

The temperature at the interface between the stator and the fluid is decided by the heat being supplied to the stator at its outer surface and the rate at which the heat is being carried away by the fluid. For a constant heat flux boundary condition, the temperature at the interface is largely decided by the rate at which the heat is being carried away by the fluid. But for a constant temperature boundary condition, even if there are differences in the rate at which heat is being carried away at the interface, the temperature is still limited by the constant temperature condition at the outer surface of the stator. Since heat transfer through the solid is essentially the same regardless of the model used, maintaining a constant temperature at the outer surface of the stator exercises a good amount of control on the temperature at the stator-fluid interface as well. But, the temperature field at regions within the flow away from the stator is bound to be different between the models because here, the temperature field is largely influenced by the rate at which heat is being carried away by the fluid.

Based on these results, we can conclude that for the special case when we are interested in the fluid-solid interface temperatures when a constant temperature boundary condition has been

specified, it might be possible to get away by running the simulation using a relatively simply turbulence model.

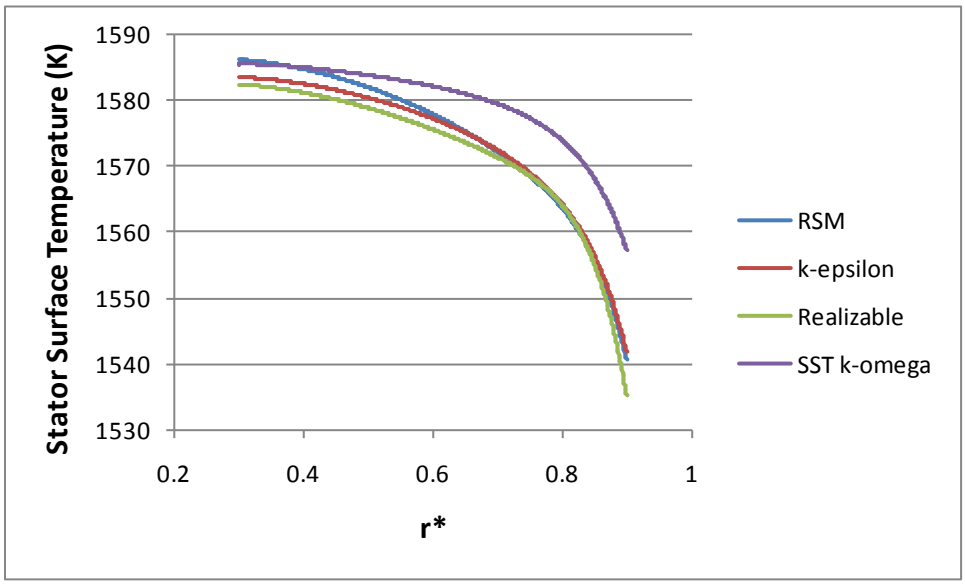

Figure 8-5 - Stator temperature vs non-dimensional radial distance for various turbulence models (High Temperature Case)

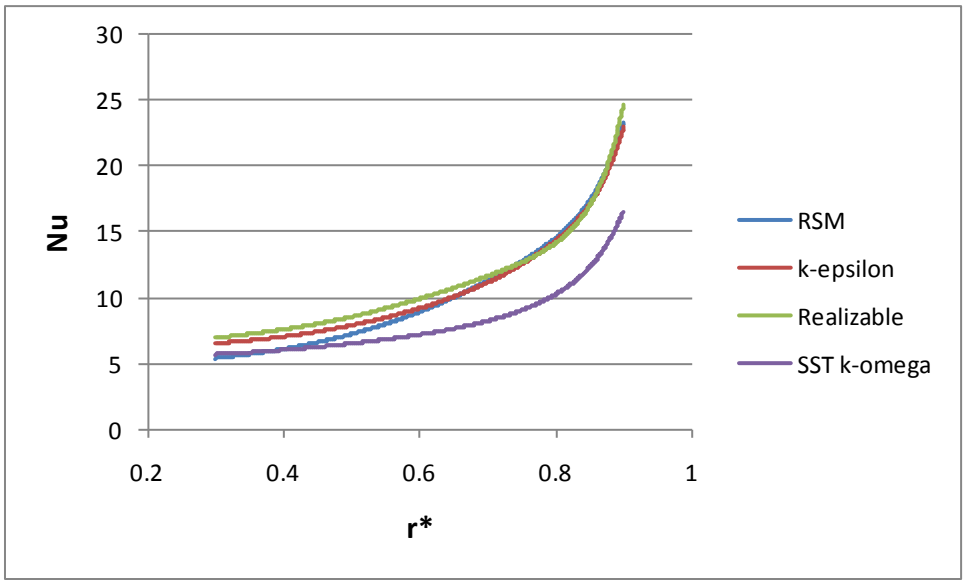

Figure 8-6 - Nusselt number at the stator surface vs non-dimensional radial distance for various turbulence models (High Temperature Case)

Chapter 9

Conclusions

The present study explored the application of a conjugate analysis to a problem involving flow and heat transfer between a rotor and a stator. It was found out that even at low temperatures, the Nusselt numbers at the stator surface vary by about 5% between the conjugate and the non-conjugate computations. The temperature distributions on the stator surface show a difference of 1% (5 K) of the non-conjugate stator surface temperature for the low temperature case and a difference of 2% (30 K) for the high temperature case. This shows the need to use conjugate approach to obtain more accurate disk temperatures and heat transfer in the cavity.

Upon comparing with experimental data, the computational results are an indicator that the Reynolds Stress Model provided by ANSYS/FLUENT is a very good computational model to model such flows. The temperature and the Nusselt number results produced from these computations indicate strongly that for modeling applications with coupled conduction and convections it is very prudent to employ a conjugate approach, especially when the temperatures involved are high.

The Iterative Conjugate Technique has been explored for the purpose of validating its usefulness as compared to the full conjugate calculation and it has been found to be successful.

Simpler turbulence models, k-ε, k-ε Realizable and SST k-ω have been found to be inadequate for swirling flows with heat transfer especially for predicting the temperature data. However, they have been found relatively satisfactory for swirling flows with heat transfer with

constant temperature boundary conditions when the interest is to obtain the fluid-solid interface temperatures and Nusselt numbers.

Chapter 10

Future Work

The present study has primarily explored centripetal flows in a rotor-stator system. Since a real turbine has both centripetal as well as centrifugal flows in it, a similar study should be carried out on a rotor-stator system with centrifugal flow. This will make the conclusions about the importance of considering conjugate heat transfer to calculate disk temperatures even more broad and comprehensive. An experiment which involves such a configuration is **[29]**. These results can be simulated using the RSM turbulence model and a comparison can be made between conjugate and non-conjugate approaches. It can then be extended to simulations at realistic turbine temperatures as has been done here.

In chapter 8 it was found out that the relatively simple turbulence models like k-ε, k-ε Realizable and SST k-ω models predicted the flow structures well, but performed badly at predicting the thermal results. It was suspected that one possible reason for this was that the turbulent Prandtl number employed by these turbulence models is wrong when applied to swirling flows with heat transfer. Thus, a study can be made to find out if this is indeed true, and if so, to obtain the correct turbulent Prandtl numbers for these turbulence models when modeling such flows. As a primer, figure 10-1 below shows the distribution of the stator temperature for four modified k-ε models. It can be seen that the results are still some way from being accurate, but the results do seem to improve by decreasing the turbulent Prandtl number.

Apart from this, more experimental work can be done with a specific aim to produce conjugate results. This is because, as it has been mentioned before, not many research efforts have been aimed towards conjugate heat transfer in rotor-stator systems. Availability of more

experimental data will help to further validate and strengthen the computational approaches to model conjugate heat transfer.

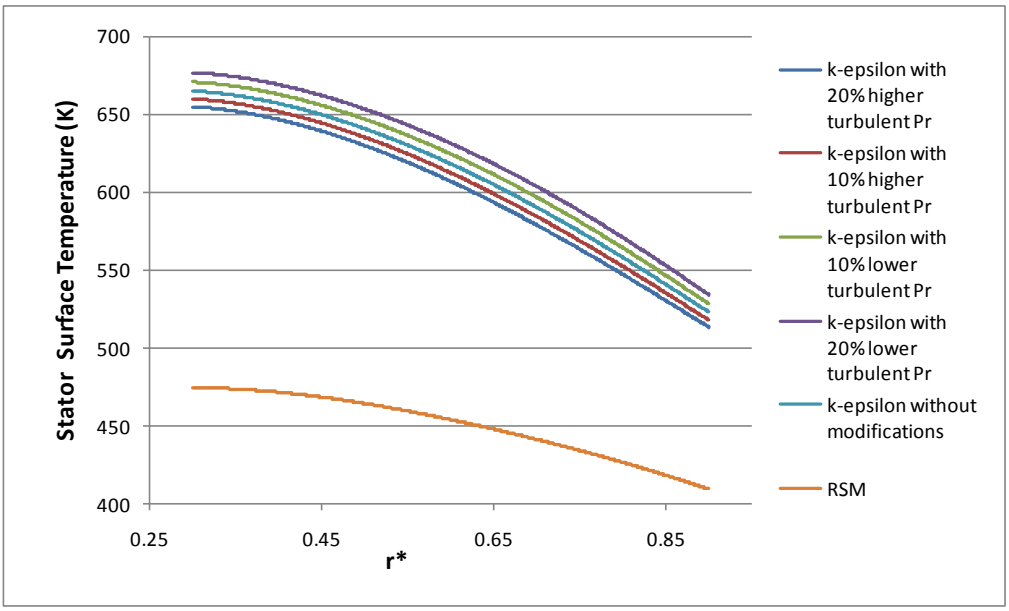

Figure 10-1 - Stator surface temperature vs non-dimensional radial distance for regular and modified k-ε models and RSM

Bibliography

[1] http://portuguesetoenglishtechnicaltranslation.com/GE-Gas-Turbines.php

[2] http://www.energy.siemens.com/hq/en/services/power-generation/product/sgt5-2000e-v94-2/lifetime-extension.htm

[3] J.W. Daily, R.E. Nece, 1960, "Chamber dimension effects on induced flow and frictional resistance of enclosed rotating disks", ASME J. Basic Engineering 82, pp. 217-232.

[4] M. Djaoui, A. Dyment, R. Debuchy, 2001, "Heat transfer in a rotor-stator system with a radial inflow", Eur. J. Mech. B – Fluids 20, pp. 371-398.

[5] S. Poncet, M.P. Chauve, R. Schiestel, 2005, "Batchelor versus Stewartson flow structures in a rotor-stator cavity with throughflow", Phys. Fluids 17 (7).

[6] E.M. Sparrow, J.L. Goldstein, 1976, "Effect of rotation and coolant throughflow on the heat transfer and temperature field in an enclosure", J. Heat Transfer 98, pp. 387-394.

[7] S. Poncet, R. Schiestel, 2007, "Numerical modeling of heat transfer and fluid flow in rotor-stator cavities with throughflow", Int. J. of Heat Mass Transfer 50, pp. 1528-1544.

[8] G.P. Beretta, E. Malfa, 2003, "Flow and heat transfer in cavities between rotor and stator disks", Int. J. Heat Mass Transfer 46, pp. 2715-2726.

[9] A. Northrop, J.M. Owen, 1988, “Heat transfer measurements in rotating-disc systems Part 2: The rotating cavity with a radial outflow of cooling air”, Int. J. Heat Fluid Flow 9 (1), pp. 27-36.

[10] J. Faragher, A. Ooi, January 2006, “Numerical Modelling of Flow and Heat Transfer in the Rotating Disc Cavities of a Turboprop Engine”, Annals of the New York Academy of Sciences, Heat Transfer in Gas Turbine Systems, volume 934, pp. 497-504.

[11] H.C. Chen, V.C. Patel, 1988, “Near-wall turbulence models for complex flows including separation”, AIAA J. 26 (6), pp. 641-648.

[12] R.P. Roy, G. Xu, J. Feng, 2001, “A study of convective heat transfer in a model rotor-stator disk cavity”, ASME J. Turbomach. 123, pp. 621-632.

[13] R. Debuchy, A. Dyment, H. Muhe, P. Micheau, 1998, “Radial inflow between a rotating and a stationary disc”, Eur. J. Mech. B – Fluids 17, pp. 791-810.

[14] K. Mangesh, S. Yavuzkurt, 2009, “Calculation of gas turbine blade temperatures using an iterative conjugate heat transfer approach”, Int. Symp. on Heat Transfer in Gas Turbine Systems 2009, Antalya, Turkey.

[15] Reby Roy K.E., B.V.S.S.S. Prasad, S. Srinivasa Murthy, 2004, “Conjugate Heat Transfer in an Arbitrary Shaped Cavity with a Rotating Disk”, Heat Transfer Engineering 25 (8), pp. 69-79.

[16] H. Iacovides, J.W. Chew, 1992, “The computation of convective heat transfer in rotating cavities”, Int. J. Heat Fluid Flow 14 (2), pp. 146-154.

[17] B.E. Launder, D.P. Tselepidakis, 1994, “Application of a new second-moment closure to turbulent channel flow rotating in orthogonal mode”, Int. J. Heat Fluid Flow 15 (1), pp. 2-10.

[18] L. Elena, R. Schiestel, 1996, “Turbulence modeling of rotating confined flows”, Int. J. Heat and Fluid Flow 17, pp. 283-289.

[19] R. Schiestel, L. Elena, 1997, “Modeling of anisotropic turbulence in rapid rotation”, Aerospace Sci. Technol. 7, pp. 441-451.

[20] ANSYS, Inc., 2009, “ANSYS/FLUENT 12.0 User’s Guide”.

[21] ANSYS, Inc., 2009, “ANSYS/FLUENT 12.0 Theory Guide”.

[22] S. Fu, B. E. Launder, M. A. Leschziner, 1987, “Modeling Strongly Swirling Recirculating Jet Flow with Reynolds-Stress Transport Closures”, Sixth Symposium on Turbulent Shear Flows, Toulouse, France, 1987.

[23] M. M. Gibson, B. E. Launder, 1978, “Ground Effects on Pressure Fluctuations in the Atmospheric Boundary Layer”, J. Fluid Mech. 86, pp. 491–511.

[24] B. E. Launder, 1989, “Second-Moment Closure and Its Use in Modeling Turbulent Industrial Flows”, Int. J. for Numerical Methods in Fluids 9, pp. 963–985.

[25] B. E. Launder, 1989, “Second-Moment Closure: Present... and Future?”, Int. J. Heat Fluid Flow 10 (4), pp. 282–300.

[26] B. E. Launder, G. J. Reece, W. Rodi, 1975, “Progress in the Development of a Reynolds-Stress Turbulence Closure”, J. Fluid Mech., 68 (3), pp. 537–566.

[27] J. C. Han, S. Dutta, and S. V. Ekkad, February 2001, “Gas Turbine Heat Transfer and Cooling Technology”, Publishers: Taylor & Francis, Inc.

[28] J. O. Hinze, 1975, “Turbulence”, McGraw-Hill Publishing Co., New York.

[29] J. -X. Chen, X. Gan, and J. M. Owen, July 1996, “Heat Transfer in an Air-Cooled Rotor-Stator System”, ASME J. Turbomachinery 118, pp. 444 – 451.